A STUDY OF QUASIMODE PARAMETRIC EXCITATIONS IN LOWER-HYBRID HEATING OF TOKAMAK PLASMAS*

E. Villalon† and A. Bers††

PFC/RR-79-13 July 1979

Submitted to Nuclear Fusion
June 1979

*One of us (E.V.) has been supported in part by grant PFPI (MEC) Spain. This work has been supported by the U.S. Department of Energy Contract (ET78-S-02-4682).

†Visiting Scientist, Research Laboratory of Electronics, M.I.T., Cambridge, MA 02139, U.S.A.

††Also, Department of Electrical Engineering and Computer Sciences, and Research Laboratory of Electronics, M.I.T., Cambridge, MA 02139, U.S.A.

Abstract

A detailed linear and nonlinear analysis of quasimode parametric excitations relevant to experiments in supplementary heating of tokamak plasmas is presented. The linear analysis includes the full ion-cyclotron harmonic quasimode spectrum. The nonlinear analysis, considering depletion of the pump electric field, is applied to the recent Alcator A heating experiment. Because of the very different characteristics of a tokamak plasma near the wall (in the shadow of the limiter) and inside, the quasimode excitations are studied independently for the plasma edge and the main bulk of the plasma, and for two typical regimes in overall density, the low (peak in density, $n_0 = 1.5 \times 10^{14}\ cm^{-3}$) and high ($n_0 = 5 \times 10^{14}\ cm^{-3}$) density regimes. At the edge of the plasma and for the low density regime, it is found that higher n_z 's ($n_z = c\ k_z/\omega$) than those predicted by the linear theory are strongly excited. Inside the plasma, the excitation of higher wave-numbers is also significant. These results indicate that a large amount of the rf-power may not penetrate to the plasma center, but will rather be either Landau-damped on the electrons or modeconverted into thermal modes, close to the plasma edge . Moreover, for sufficiently high peaks in density it is found that all the rf-power is modeconverted before reaching the plasma center. Inside the plasma the power density of the excited sideband fields is shown to be always very small in comparasion with their excitation at the plasma edge.

I. Introduction

In the heating of tokamaks with rf-power near the lower-hybrid frequency, the driven fields can act as a pump for parametric instabilities. The lower-hybrid fields are principally electrostatic, and are characterized by a frequency $\omega_{\ell h} = \frac{\omega_{pi}}{(1 + \omega_{pe}^2/\Omega_e^2)^{1/2}}$, and wavevectors $k_\parallel$ (parallel to the magnetic field $\vec{B}$) and $k_\perp$ (perpendicular to $\vec{B}$) such that $\frac{k_\parallel}{k_\perp} \ll 1$. The quasimode type of parametric instabilities consist in the excitation of a lower-hybrid sideband wave from the background noise level through low frequency fluctuations in the plasma. The power levels in current tokamak experiments [1] usually exceed the thresholds for this parametric instability to occur, and these experiments, as well as several other tokamak heating experiments over the past few years [2], all indeed show the presence of such excitations. This has provoked extensive studies of these processes in the last few years. The original, linear analysis of the temporal evolution of this instability [3] has been recently extended and complemented with extensive numerical computations [4]. This instability is however a convective one and its spatial evolution in a pump of finite spatial extent is more relevant. The linear spatial evolution, including group velocities along and transverse to the magnetic field, for a constant pump of a finite spatial extent is discussed in Ref. [5]. The nonlinear effects of pump depletion have been formulated and discussed in general terms, in Refs. [6,7]. Other nonlinear saturation effects have also been invoked; these relate mainly to models of temporal cascading in which the excited lower-hybrid sidebands are treated in the random-phase approximation [8]. We shall not consider these here any further, especially since the physically important nonlinear evolution is a spatial one. In spite of the broad attention that this problem has recieved, there are still many unresolved questions regarding the relevance and physical consequences of these parametric excitations in today's tokamak experiments. More specifically, it is of interest to know how physical effects like pump depletion will scale with density and temperature; what the excited spectrum will be in terms of

change with changes in the density and temperatures. We present results that attempt to answer these questions and give us a better insight into the effects that these parametric processes have in plasma heating.

Our plasma model is a two-dimensional one, the x-direction is the direction of the plasma inhomogenities (i.e. density, temperatures, and toroidal magnetic field inhomogenities), and the z-direction is in the direction of the toroidal magnetic field. We apply the theoretical results to parameters relevant to the recent Alcator A heating experiment [1].

We first start with a detailed analysis of the linear theory (Sects. II and III). The low frequency fluctuations are due to both electrons and ions. In the previous works, it was commonly assumed that the quasimode excitation due to scattering off ions is neglegible under the approximation $T_e \gg T_i$. This is never true for tokamak devices, and we shall see that scattering off ions give important modifications to the excited spectrum. We distinguish between two different spatial regions , the plasma edge (in the shadow of the limiters [9]) and the main bulk of the plasma. We also make a comparative study between the two different regimes, of low and high densities. The low density regime correspond to a peak density of about $n_0 = 1.5 \times 10^{14}\ cm^{-3}$, and the high density regime to a peak density around $n_0 = 5 \times 10^{14}\ cm^{-3}$. The plasma edge is characterized by a large drop in density and temperatures inside the shadow of the limiter [9]. Parametric excitations are particularly strong here, and the characteristics of the excited spectrum differ importantly from the ones found inside the plasma.

Nonlinear calculations are carried out in Sections IV and V . The linear analysis presented in the preceding sections then acquires its complete physical meaning. We study how the pump is depleted at the edge and in the plasma. Pump depletion is going to have important consequences in plasma heating, since it may change completely the characteristics of the power spectrum entering inside the plasma. These changes are mainly affecting the wave-number spectrum and the power density. We find that at the edge of the plasma, strong nonlinear excitations of higher n_z 's may take place that will change radically the power spectrum and the amount of power penetrating into

the plasma. Depletion in the plasma depends critically on the density regime we are considering. This becomes larger with increasing density. Inside the plasma the excited sideband spectrum has a field amplitude which, in general, is never comparable to the pump amplitude. The modified wave-number spectrum also plays an important role in determining how much of the total power penetrates up to the center of the plasma. All the results are summarized in Sect. VI.

Finally, it should be remarked that there are a variety of nonlinear phenomena that can be operative in lower-hybrid heating of a tokamak-type plasma. In this paper we have focused on the quasimode parametric excitations. Other parametric excitations and selfmodulation effects, especially at the plasma edge, may also have important consequences in lower-hybrid heating. Their interaction with quasimode excitations is beyond the scope of this paper.

II. Linear Theory, Spatial Growth Factor

The linear steady-state evolution of a sideband field $\vec{E}_1$ driven by a pump field $\vec{E}_0$ which decays via nonlinear damping on electrons or ions is given by [6],

$$\vec{v}_1 \cdot \nabla E_1^2 = \left(C(x) E_{0\ell}^2(x)\right) E_1^2 \tag{1}$$

where $\vec{v}_1$ is the group velocity of the sideband, $C(x)$ is the coupling coefficient, $E_{0\ell}^2(x)$ is the magnitude of the pump field as described by the linear equations, and E_1^2 is the magnitude of the excited sideband field. The coordinate x is in the direction of the spatial inhomogeneities and is normalized to the slab half-width a. By integrating Eq. (1) along the group velocity trajectory of the sideband field, one finds the spatial growth factor (Fig. 1)

$$\Gamma(x) = a \int_{x_1}^{x} \frac{\gamma(x')}{v_{1x}(x')}\, dx' \tag{2}$$

where $\gamma(x) = C(x)\, E_{0\ell}^2(x)/2$ is the temporal growth rate,

$$\gamma(x) = \frac{\mu^2}{8} \frac{\omega_{\ell h}^2}{\omega_0^2} \sin^2(\phi)\left(1 - \frac{\omega}{\omega_1}\frac{k_{1z}}{k_z}\right) k^2 \lambda_{De}^2\, Im\left(\frac{(1+\chi_i)\chi_e}{1+\chi_i+\chi_e}\right) \tag{3}$$

$\omega_{\ell h}^2 = \dfrac{\omega_{pi}^2}{1 + \omega_{pe}^2/\Omega_e^2}$, ω_0 and ω_1 are the pump and sideband frequencies, $\omega = \omega_0 - \omega_1$ is the frequency of the quasimode, $\vec{k}_0$ and $\vec{k}_1$ the pump and sideband wavevectors, $\vec{k} = \vec{k}_0 - \vec{k}_1$, and $\cos(\phi) = \dfrac{k_{1x}}{k_{1\perp}}$. We are assuming a uniform pump electric field in the y-direction so that $\vec{k}_0 = (k_{0x}, k_{0z})$. For this pump field, one finds,

$$\mu^2 = \left(\frac{E_{0\ell}}{B c_s}\right)^2 = \frac{p_0}{n T_e v_{Te}} \frac{\omega_{pi}^2}{\Omega_i^2} \frac{k_{0z} v_{Te}}{\omega_0} \frac{1}{|x|} \sqrt{-\frac{K_{0\parallel}}{K_{0\perp}^3}} \tag{4}$$

p_0 is the rf-power density, n and T_e denote the local density and temperature (in energy units) and $K_{0\parallel}$, $K_{0\perp}$ are elements of the cold plasma dielectric tensor for the frequency ω_0.

Let us denote by the subscripts I and R the imaginary and real parts, respectively, of the susceptibilities of the low frequency mode $\chi_{e,i}(\vec{k}, \omega)$, where the subscripts e and i stand for,

respectively, "electron" and "ion", then

$$Im\left(\frac{(1+\chi_i)\chi_e}{1+\chi_i+\chi_e}\right) = \frac{\chi_{eR}^2\,\chi_{iI} + \chi_{eI}[(1+\chi_{iR})^2 + \chi_{iI}(\chi_{eI}+\chi_{iI})]}{(1+\chi_{iR}+\chi_{eR})^2 + (\chi_{eI}+\chi_{iI})^2} \quad . \tag{5}$$

We see that the scattering off the low frequency mode can be due, in principle, to both electrons and ions. We are now interested in getting explicit forms for χ_e and χ_i. For electrons one has that $\omega \ll \Omega_e$ and $\left(\frac{k_\perp v_{Te}}{\Omega_e}\right)^2 \ll 1$, which immediately leads to [10],

$$\chi_e = \frac{1}{k^2\lambda_{De}^2}\left\{1 + \frac{\omega}{\sqrt{2}|k_z|v_{Te}}\,Z\left(\frac{\omega}{\sqrt{2}|k_z|v_{Te}}\right)\right\} \tag{6}$$

In previous works [3 - 7], it was commonly assumed that $T_e \gg T_i$, and thus that $|\chi_i| \gg |\chi_e|$. Under these conditions Eq. (5) becomes equal to

$$\chi_{eI} = \frac{1}{k^2\lambda_{De}^2}\sqrt{\frac{\pi}{2}}\,\frac{\omega}{|k_z|v_{Te}}\,exp(-\frac{\omega^2}{2k_z^2 v_{Te}^2}) \tag{7}$$

implying that the scattering is only due to electrons. This, we find, is never true for tokamak-type plasma parameters where, in fact, one finds $T_e \simeq T_i$ and ion contributions to the scattering is important.

For lower-hybrid heating of typical tokamak plasmas one finds, that the low frequency quasimode excitation in the plasma can span several ion cyclotron harmonics. In addition one finds, that inside the plasma, $\Lambda_n(\beta_i) = I_n(\beta_i)\,exp(-\beta_i)$ is usually small, since $\beta_i = \left(\frac{k_\perp v_{Ti}}{\Omega_i}\right)^2$ is greater than 1. This means that the contribution of the corresponding n will not be appreciable unless the Z-function contribution is large. Let us fix ω and x and define $r(x,\omega)$ as the closest integer to $\frac{\omega}{\Omega_i(x)}$, we thus approximate χ_{iR} by

$$\chi_{iR} = \frac{1}{k^2\lambda_{Di}^2}\left\{1 + \frac{\omega}{\sqrt{2}|k_z|v_{Ti}}\sum_{n=r-1}^{r+1} Z_R\left(\frac{\omega - n\Omega_i}{\sqrt{2}|k_z|v_{Ti}}\right)\Lambda_n(\beta_i)\right\} \tag{8}$$

where we have reduced the infinite sum in all the cyclotron harmonics ($n = -\infty, \ldots 0 \ldots, \infty$) to only three terms, and Z_R denotes the real part of the Z-function. For the imaginary part of χ_i one has,

$$\chi_{iI} = \frac{1}{k^2\lambda_{Di}^2}\sqrt{\frac{\pi}{2}}\,\frac{\omega}{|k_z|v_{Ti}}\,exp\left(-\frac{(\omega - r\Omega_i)^2}{2k_z^2 v_{Ti}^2}\right)\Lambda_r(\beta_i) \quad . \tag{9}$$

The behavior of the real and imaginary parts of Z with respect to its argument, and the fact that $\frac{|k_z|v_{Ti}}{\Omega_i} \ll 1$, lead to only large values of Z in a narrow interval of the frequency spectrum around the point $\omega = n\Omega_i$; this interval being even narrower for the imaginary part of Z, for which one can say that it is only different from zero when ω is very close to $r\Omega_i$. Thus, for fixed x and ω, we need only to take account of the closest harmonics as expressed in Eqs. (8) and (9). When $\omega < \Omega_i$, the main contributing term is for $n = 0$ which turns out to be always inappreciable for $|x| < 1$, since it requires $\frac{\omega}{\omega_0} \simeq \frac{|k_z|v_{Ti}}{\omega_0} \ll 1$ and thus that ω_1 be very close to ω_0 where the growth factor is always small. For this situation, we can approximate χ_i by the real quantity: $\chi_i = \frac{1}{k^2\lambda_{Di}^2}$.

We note that the growth factor of the interaction is only appreciable when electron Landau damping for the quasimode is important, i.e. $\frac{\omega}{|k_z|v_{Te}} < 3.5$. The ion-cyclotron harmonic dependence of the quasimode gives important modifications to the growth factor as a function of frequency. This can be appreciated from the following: let us assume that $\chi_{el} \simeq 0$, (i.e. $\frac{\omega}{|k_z|v_{Te}} > 3.5$). Equation (5) now becomes

$$k^2\lambda_{De}^2 \, Im\left(\frac{(1+\chi_i)\chi_e}{1+\chi_i+\chi_e}\right) \simeq \frac{k^2\lambda_{De}^2 \chi_{eR}^2 \chi_{il}}{(1+\chi_{iR}+\chi_{eR})^2 + \chi_{il}^2} \tag{10}$$

where $\chi_{eR} = \frac{-1}{k^2\lambda_{De}^2}\left(\frac{k_z v_{Te}}{\omega}\right)^2$ and $k^2\lambda_{De}^2 \ll 1$. Equation (10) is always very small, even if $\omega = n\Omega_i$, since $k^2\lambda_{De}^2 |\chi_{eR}|$ is small. The only exception is when, for certain $\omega \simeq n\Omega_i$, $(1+\chi_{iR}) \simeq -\chi_{eR}$, Eq. (10) then reducing to $k^2\lambda_{De}^2 \frac{\chi_{eR}^2}{\chi_{il}}$ which can give large growth factors if $\chi_{il} \ll (1+\chi_{iR})^2$. However, for $1 + \chi_i + \chi_e \simeq 0$, the low frequency is no longer a quasimode but a true mode; thus the interaction becomes a resonant three wave interaction and is no longer described by the quasimode equations, Eq. (1). Here, we shall not pursue such resonant interactions.

To calculate Γ as a function of ω_1 for a fixed x and a given pump frequency ω_0 (e.g. $\omega_0 = 2.45\ Ghz$ for Alcator A), we shall proceed by first choosing some values for $n_{0z} = \frac{ck_{0z}}{\omega_0}$ and $n_{1z} = \frac{ck_{1z}}{\omega_1}$. The parameter n_{0z} is really fixed by the rf-power spectrum distribution which we shall specify in the next section. Besides there are two physical conditions limiting the range of variation

for n_{0z} and n_{1z}: a) Pump and sideband are fluid like waves, that is they cannot be electron Landau damped ($\frac{\omega_0}{k_{0z}v_{Te}} > 3.5$ and $\frac{\omega_1}{k_{1z}v_{Te}} > 3.5$); this gives the upper bound

$$n_{0,1\,z} < \frac{1}{3.5}\ \frac{c}{v_{Te}} \tag{11}$$

b) The lower bound is given by the requirement $k^2_{0,1\,\perp} > 0$ in the region where the interaction takes place.

The excited frequency spectrum is found by using the condition of strong electron Landau damping of the quasimode $\frac{\omega}{|k_z|v_{Te}} < 3.5$,

$$\frac{\alpha_z \pm 3.5}{\beta_z \pm 3.5}\ \frac{\beta_z}{\alpha_z} < \frac{\omega_1}{\omega_0} < 1 \tag{12}$$

where $\alpha_z = \frac{\omega_0}{k_{0z}v_{Te}}$, $\beta_z = \frac{\omega_1}{k_{1z}v_{Te}}$, and we assume that $k_{1z} > 0$. The minus sign is taken when $\alpha_z < \beta_z$ and the plus when $\alpha_z > \beta_z$. Once we choose n_{0z}, n_{1z} and ω_1, we can solve for $k_{0\perp} = k_{0x}$ and $k_{1\perp}$ using the lower-hybrid dispersion relation corrected for finite temperatures effects,

$$a\,k^4_\perp + (b\,k^2_z - K_\perp)k^2_\perp + c\,k^4_z - k^2_z\,K_\parallel = 0 \tag{13}$$

where a, b and c are given elsewhere [11].

Let us now determine the lower limit of the integral x_1, in Eq. (2), for a given x. Denoting by $\vec{v}_0$ the group velocity of the pump field, one finds

$$a\int_x^{x_1} \frac{v_{0z}}{v_{0x}}\,dx' - \frac{L}{2} = \frac{L}{2} + a\int_x^{x_1} \frac{v_{1z}}{v_{1x}}\,dx' \tag{14}$$

where L is the width of the pump propagation cone. It turns out that, for $|x| < 1$, x_1 is always very close to x which allows one to approximate

$$\Gamma(x) = \frac{\gamma(x)}{v_{1x}}\ \frac{L}{\left(\frac{v_{1z}}{v_{1x}} - \frac{v_{0z}}{v_{0x}}\right)} \tag{15}$$

This growth factor can now be maximized with respect to the angle ϕ. Γ dependencies on ϕ come through $\gamma(x)$ which behaves like $sin^2(\phi)$ (see Eq. (3)), and through

$$v_{1x} = -\frac{\omega_1}{k_{1z}} \frac{\cos(\phi)}{1 + \frac{\omega_{pe}^2}{\Omega_e^2}} \sqrt{\frac{K_{1\perp}^3}{-K_{1\parallel}}} \tag{16}$$

$$\frac{v_{1z}}{v_{1x}} - \frac{v_{0z}}{v_{0x}} = -\left(\frac{1}{\cos\phi} \sqrt{-\frac{K_{1\parallel}}{K_{1\perp}}} - \sqrt{-\frac{K_{0\parallel}}{K_{0\perp}}} \right) \tag{17}$$

$K_{1\perp}$ and $K_{1\parallel}$ are elements of the cold plasma dielectric tensor for the frequency ω_1. Putting these together in Eq. (15), leads to the total angular dependencies of the growth factor Γ, which can be easily maximized to obtain

$$\cos(\phi) = \sqrt{\frac{(-K_{1\parallel})}{K_{1\perp}} \frac{K_{0\perp}}{(-K_{0\parallel})}} - \sqrt{\frac{(-K_{1\parallel})}{K_{1\perp}} \frac{K_{0\perp}}{(-K_{0\parallel})} - 1} \tag{18}$$

In the computations we shall only consider the maximum growth factor with respect to ϕ. We note that in this section and for the rest of the paper, we limit ourselves to the case $k_{1z} > 0$, which is maximized according with Eq.(18) for $v_{1x} < 0$. This case represents waves travelling toward the center of the plasma. When $k_{1z} < 0$, Eq.(15) is maximized with respect to $\cos(\phi)$, for $v_{1x} > 0$ representing waves travelling toward the plasma edge. We are not considering this last possibility since the results will be similar in both cases, and only the direction of propagation is reversed. However, one has always to remember that when parametric excitations become strong and the rf-power is transferred to the excited waves, a large part of this power will travel down to the plasma edge. In general, we find that $\cos(\phi) > 0$ ($k_{1z} > 0$)and as $\omega_1 \to \omega_0$, $\cos(\phi) \to 1$ (i.e. $k_{1\perp} \to k_{1x}$ and $k_{1y} \to 0$). It should be noted that in the temporal evolution of the instability, the temporal growth factor, given by Eq.(3), maximizes with respect to ϕ when $\cos(\phi)$ is zero, that is when $k_{1\perp} = k_{1y}$ and $k_{1x} = 0$ representing waves which will never get into the center of the plasma.

III. Linear Theory, Calculations

A. Inside the Plasma

In our computer calculations we consider a D_2-plasma and take the density, temperatures and toroidal magnetic field to be spatially inhomogeneous obeying the following profiles, consistent with measurements on Alcator A [12]

$$n = n_0\left(1 - \frac{x^2}{1.47}\right)^{3/2} \tag{19}$$

$$T = T_0\, e^{-2x^2} \tag{20}$$

$$B = B_0\,(1 - \frac{x}{5.68}) \tag{21}$$

where n_0, T_0 and B_0 are the density temperatures and magnetic field values at the center of the plasma, $x = 0$. We shall take B_0 fixed at 60 KG, and consider two typical values for the peak density, $n_0 = 1.5 \times 10^{14}$, and $5 \times 10^{14}\ cm^{-3}$. The corresponding peaks in temperatures are, for the low density regime: $T_{e0} = 1.3\ Kev$, $T_{i0} = 0.75\ Kev$, and for the high density regime: $T_{e0} = 1.15$ Kev, $T_{i0} = 0.68\ Kev$. The accessible n_z's are $n_{za} = 1.6$ and 2, respectively.

As an example we apply the theory previously outlined, to the experimental characteristics of Alcator A. We use the maximum applied rf-power as 80 Kw, driven at the plasma wall through a two waveguide array, each of width $\frac{w}{2} = 1.25\ cms$, and height $h = 8\ cms$. Reflection back into the waveguides, reduces the available power by 20%. According to linear theory [13, 14], from the remaining 64 Kw, about 35 to 40% is below accessibility. This power is fed to surface mode fields that remain near the plasma wall, and never penetrates in the main bulk of the plasma. Let us restrict ourselves to the propagation cone, $k_{0z} > 0$. Following linear theory, the accessible power is distributed within the wave-numbers $n_z = 2$ to 5 as follows: between $n_z = 2$ and 3 there is an average of approximately 7.5 Kw, between $n_z = 3$ and 4 5.5 Kw, and between $n_z = 4$ to 5 3 Kw;

in addition there are about 2 Kw of power beyond $n_z = 5$. The total power in a resonance cone will be taken as approximately 17.5 Kw. We are modeling this power distribution with the function $\frac{2}{\pi}\frac{c}{\omega_0}\frac{P_0(x)}{L}\frac{\sin^2\left[(n_z - n_{0z})A\right]}{(n_z - n_{0z})^2}$, where $A = \frac{\omega_0}{2c} \times L$, and $L(x)$ is the width of the pump cone which depends on the amount of power, $P_0(x)$, penetrating to a certain point in the plasma.

In addition to accessibility which limits the power penetration into the plasma, modeconversion of the pump electric field [11] will also restrict the amount of power getting to the plasma center. In Fig. 2 we show how the different wave-numbers n_{0z} are modeconverted as they propagate into the plasma, for the two regimes of low (Fig. 2A) and high (Fig. 2B) densities. We see that for the low density regime, all the linear power spectrum reaches in the plasma center. In the high density regime, and for $x < 0.5$, only that part of the spectrum between the wave-numbers, $n_z = 2$ to 3, penetrates. These considerations, and the n_z power spectrum distribution predicted by the linear theory, allow us to make the following estimations : Inside the plasma, $x < 1$ for the low density regime and $0.5 < x < 1$ for the high density regime, we will assume for linear calculations that $P_0 \sim 17.5\ Kw$ and the pump spectrum is centered at $n_{0z} = 3.5$, with $L \sim 1.3\ w$. For the high density regime and for $x < 0.5$, one has, because of modeconversion, $P_0 \sim 7.5\ Kw$, the spectrum being centered at $n_{0z} = 2.5$, with $L \sim 4w$, i.e. the propagation cone is four times larger than the waveguides width. In any of the former cases, the power density is obtained by dividing the rf-power available by the area of the corresponding pump cone. We note that Γ is independent of the pump width as can easily be seen from Eqs.(3), (4) and (15).

In Fig. 3 we are representing Γ as a function of the frequency spectrum for the two different peaks in density, and for two different positions in the plasma, near the edge, $x = 0.75$, and near the center $x = 0.25$. The power distribution fixes $n_{0z} = 3.5$ except for $n_0 = 5 \times 10^{14}\ cm^{-3}$ and $x = 0.25$, where as explained before $n_{0z} = 2.5$. The power available is 17.5 Kw except for the high density regime and $x = 0.25$, where due to modeconversion, the power available is 7.5 Kw. We have chosen $n_{1z} = 2$ in Figs. 3A and 3B, and $n_{1z} = 5$ in Figs. 3C and 3D. Comparing Figs. 3A and 3B we see that the spatial growth factor increases very rapidly with density due to the WKB

enhancement and cylindrical focusing factor of the pump field; we ignore the focusing factor at about half-way to the center of the plasma. We also note that v_{1x} gives an additional WKB-type of enhancement for Γ (see Eqs. (15) and (16)). Moreover we find that both v_{0x} and v_{1x} are small, and that pump and sideband move parallel to the magnetic field: $|\frac{v_{1z}}{v_{1x}}| > |\frac{v_{0z}}{v_{0x}}| > 30$, and they reach values of the order of 100 at the highest densities. The number of resonant peaks observed in the calculations, vary with the width of the excited spectrum, which depends on n_{0z}, n_{1z} and x, see Eq.(12) . When n_{0z} and n_{1z} are close in value, the number of resonant harmonics, and the width of the excited spectrum, are smaller than when they are far from each other. This is illustrated in Figs. 3A and 3C where the density is the same but n_{1z} is different. We also note that Γ increases with increasing n_{1z}, this being due to the v_{1x}-dependency upon n_{1z} as shown in Eq. (16). We shall discuss later on the important consequences of this fact. Figures 3B and 3D also differ in the value of n_{1z}. As the density is already too high, sideband fields with high n_{1z}'s can only be excited close to the edge of the plasma, $x \sim 0.75$, as shown in Fig. 3D. This is due to modeconversion of the excited fields. Modecoversion for the pump electric field was shown to occur at different n_z's for different peaks in density (see Fig. 2). Similarly, the values that n_{1z} and ω_1 can take for a given density are also restricted by modeconversion. As the density increases, ω_1 has to be closer to ω_0 and n_{1z} closer to accessibility in order for Eq.(13) to give a real $k_{1\perp}$. For example, in Fig.3D and for $x < 0.5$, no sideband fields can be excited due to n_{1z} being too large ($n_{1z} = 5$) for such densities. Similar restrictions due to modeconversion of the sideband are found in Fig. 3B, for $x = 0.25$ and $\omega_1/\omega_0 < 0.96$. In Fig. 4, we are representing Γ for the low density case at $x = 0.75$, and taking $n_{1z} = 12$ and $n_{0z} = 6.5$. The reasons why we have shifted the pump spectrum toward higher n_z's, will be explained in the next sections. What we want to notice here, is that Γ also increases linearly with n_{0z} (see Eq. (4)), and that parametric excitations for such high values of n_{1z} can only take place close to the edge ($x \sim 0.75$).

The nodes of the growth factor occur when ω is near $n\,\Omega_i$, $\chi_{il} = 0$ and $(1 + \chi_{iR}) = 0$. As pointed out, χ_{il} is only different from zero in a tiny region around $\omega = n\,\Omega_i$, thus for $\omega \neq n\,\Omega_i$ we can take

$$Im\left(\frac{(1+\chi_i)\chi_e}{1+\chi_i+\chi_e}\right) = \chi_{el}\,\frac{(1+\chi_{iR})^2}{(1+\chi_{iR}+\chi_{eR})^2+\chi_{el}^2} \qquad (22)$$

which becomes zero for $\chi_{iR} = -1$. As we are considering an inhomogeneous magnetic field, the position of the resonant ω will change in space and so will also the the positions of the growth factor nodes. This means that for a fixed ω_1, there will be regions in x where the pump and sideband are coupled, and others where the coupling is very small. The maximum values for Γ between nodes, are approximately given by the condition: $1+\chi_{iR}+\chi_{eR} \sim 0$ (except when χ_{eR} is very small and then $1+\chi_{iR}$ becomes zero simultaneously). We note that the function $1+\chi_{eR}+\chi_{iR}$ has a zero between each two harmonics, these zeros are very close to those of $1+\chi_{iR}$. At these zeros, Eq. (22) behaves like $\frac{(1+\chi_{iR})^2}{\chi_{el}}$. When χ_{el} is small, that is when ω is far away from the main bulk of the electron damping (e.g. $\frac{\omega}{|k_z|\,v_{Te}} > 3$ or $\frac{\omega}{|k_z|\,v_{Te}} < 0.5$), the zeros of $1+\chi_{eR}+\chi_{iR}$ can lead to singularly high values for Γ, as can be observed in the different figures presented. These singular values correspond to frequencies fulfilling, $1+\chi_i+\chi_e \sim 0$, which, as remarked before, is the transition condition between a well defined low frequency mode and a quasimode (i.e. one for which $1+\chi_i+\chi_e \neq 0$). Our formulation is no longer valid here, and such values of Γ should not be considered as reliable; they would have to be calculated from a resonant three-wave interaction formulation.

B. The plasma edge

Let us now study in detail the quasimode parametric excitations in a special region of the plasma situated in the shadow of the limiters of the tokamak. This region is characterized by a large drop in density and temperatures [9]. The drop in density can still be approximately described by Eq. (19), taking $|x| \sim 1$. The corresponding drop in temperatures is about a factor 10 larger than the one prescribed by Eq. (20) taking $|x| \sim 1$. This leads to very high values of μ^2, given by Eq. (4), and thus to very large values for the spatial growth factor. We are going to explore the regimes of low ($n_0 = 1.5 \times 10^{14}\ cm^{-3}$) and high ($n_0 = 5 \times 10^{14}\ cm^{-3}$) central densities. According to the experimental results in Ref. [9], for the high density regime one finds at the edge: $n \sim 6.7 \times 10^{13}\ cm^{-3}$ and $T_e \sim 10\ ev$; for the low density regime one has: $n \sim 2 \times 10^{13}\ cm^{-3}$, and $T_e \sim 10\ ev$ The toroidal magnetic field is about 50 KG and the ratio between electron and ion temperatures will be assumed to be the same as in the center of the plasma, so that $T_i \sim T_e$ It should be remarked that the ion temperature in the shadow of the limiter was not measured in Ref. [9]. The possibility exists that $T_e \gg T_i$ and hence the parametric excitation could be a resonant one involving ion-cyclotron and, or, ion acoustic waves. Here we assume $T_e \sim T_i$ for which case the quasimode excitation is dominant. At the plasma edge, $x \sim 1$, the available power in a cone will be assumed to be 32 Kw, centered around $n_{0z} = 3$, and L taken to be just the width of the waveguides, $w = 2.5\ cm$. We remark that by taking into account part of the power not accessible to the plasma, we consider the possibility that by decaying into higher n_z's it might become accessible and then penetrate into the plasma.

We have already commented that Γ increases linearly with n_{1z}, this will have important consequences in this region of the plasma. The parameter n_{1z} is restricted by the condition of Eq. (11), and by modeconversion. At the edge, due to the large drop in temperatures, n_{1z} can vary from 1 to 50. Hence, the growth factors will increase to enormous values for the higher n_{1z}'s. In Fig. 5, we represent Γ as a function of ω_1 for the two regimes and for differents values of n_{1z}; for the low density regime (Fig. 5A) we take $n_{1z} = 6$ and 8, while for the high density regime (Fig. 5B),

we take n_{1z} = 1.5 and 4. We see that similar values for Γ are obtained for different values of n_{1z} as one considers the regimes of low or high densities. As the density decreases, n_{1z} has to become larger in order to keep Γ as large as when the density is high and n_{1z} small. We also note that the frequency spectrum is much narrower than the one usually found inside the plasma; this is also due to T_e being small: The pump spectrum is centered at n_{0z} = 3, implying $\alpha_z = \frac{\omega_0}{k_{0z} v_{Te}} \sim 70$, and the lower limit of Eq.(12) becomes now approximately equal to, $\frac{\beta_z}{\beta_z \pm 3.5}$. Thus, if $n_{1z} < 10$, that is if $\beta_z = \frac{\omega_1}{k_{1z} v_{Te}} \gg 3.5$, one gets that $\frac{\omega_1}{\omega_0}$ is very close to 1. Given these large growth factors one can conclude, and we shall corraborate it in the nonlinear calculations, that the pump will be completely depleted in the limiter region. The excited sideband fields have a frequency close to the pump frequency, but the wave-number spectrum may be very different from the initial linear spectrum.

It should also be noted that in Fig. 5 the narrow regions of growth factor very close to the pump frequency ω_0, can be attributed to ion-acoustic quasimode interactions, i.e. those driven by ion-Landau damping of the quasimode, these giving rise to the peak very near ω_0. However at such small frequencies, it may be that our quasimode formulation is not the most appropiate one since $\chi_{el} \sim 0$, and, again, a resonant three-wave interaction with ω very small should be carry out.

Regarding the computational methods used in this region, we have to remark that as the plasma parameters are quite different from the ones inside the plasma $|x| < 1$, the discussion presented in Sect. I to derive Eqs. (8) and (9) is no longer valid here. In fact, now $\beta_i = \left(\frac{k_\perp v_{Ti}}{\Omega_i}\right)^2 \gtrsim 1$, and for a given ω, we cannot be sure that the main contributing harmonic is the closest to $\omega = n\ \Omega_i$, since the Bessel functions are not as small as they were before. In all the calculations we have used a sufficient number of harmonics to obtain accurate results.

IV. Nonlinear Depletion

The depletion of the pump field and the nonlinear evolution of the excited sideband field, are described by the following nonlinear equations [6]

$$\left(v_{0x}(x)\frac{\partial}{\partial x} + v_{0z}(x)\frac{\partial}{\partial z}\right)E_0^2 = -C(x)E_0^2 E_1^2 \tag{23}$$

$$\left(v_{1x}(x)\frac{\partial}{\partial x} + v_{1z}(x)\frac{\partial}{\partial z}\right)E_1^2 = C(x)E_0^2 E_1^2 \quad . \tag{24}$$

Equations (23) and (24) have been obtained through a WKB mode analysis assuming the plasma to be weakly inhomogeneous.

For a homogeneous medium Eqs. (23) and (24) admit the exact solutions [15]

$$\psi_0 = -\frac{\partial}{\partial\tau}(\ell n\,(S(\theta) - T(\tau))) \tag{25}$$

$$\psi_1 = +\frac{\partial}{\partial\theta}(\ell n\,(S(\theta) - T(\tau))) \tag{26}$$

where $\psi_0 = \dfrac{C E_0^2}{v v_{1x}}$, $\psi_1 = \dfrac{C E_1^2}{v v_{0x}}$, $v = \dfrac{v_{0z}}{v_{0x}} - \dfrac{v_{1z}}{v_{1x}}$, $\theta = z - a\displaystyle\int_1^x \frac{v_{1z}}{v_{1x}}\,dx'$ and $\tau = -(z - a\displaystyle\int_1^x \frac{v_{0z}}{v_{0x}}\,dx')$. We shall assume a finite uniform extended pump at $x = 1$, $A_0 = \psi_0(x = 1, |z| < w/2)$, and denote by $A_1 = \psi_1(x = 1)$ the noise level. The functions $S(\theta)$ and $T(\tau)$ are uniquely specified in terms of A_0 and A_1 for the two different regions: $|\tau| < L/2$, $|\theta| < L/2$ (region I) and $|\tau| < L/2$, $\theta < -L/2$ (region II), see Fig. 1, and their analytic expressions can be found in [15].

For an inhomogeneous plasma we shall also describe the dynamics of the interaction through Eqs. (25) and (26), but now A_0 and A_1 become slowly-varying functions of the inhomogeneity coordinate x.

$$A_0(x) = \frac{C(x)}{v(x)}\,\frac{E_{0\ell}^2(x)}{v_{1x}(x)} \quad . \tag{27}$$

$$A_1(x) = \frac{C(x)}{v(x)} \frac{E_{1\ell}^2(x)}{v_{0x}(x)} \tag{28}$$

where $E_{0\ell}(x)$ and $E_{1\ell}(x)$ are the pump and sideband electric field as described by the linear equations,

$$E_\ell^2 = \frac{2}{\varepsilon_0} \frac{p}{|x|} \cos(\phi) \frac{k_z}{\omega} \sqrt{\frac{-K_\parallel}{K_\perp^3}} \tag{29}$$

$\cos(\phi) = \frac{k_x}{k_\perp}$, p is the power density which, for the pump, has already been specified in the former sections, and for the sideband we assume $p_r = \frac{p_1}{p_0} = 5 \times 10^{-4}$. Equations (25), (26) and (27), (28) describe the evolution of the interaction in a WKB sense, that is if this evolution is faster than the variation of plasma parameters with x.

As a measure of power depletion we compute the average of the square pump electric field along the width of the resonance cone, and the sideband field coming out from the resonance cone (i.e. at $\tau = -L/2$). For $(1 - x) > \Delta x_w$, where $\Delta x_w = \frac{w/a}{|v_{1z}/v_{1x} - v_{0z}/v_{0x}|}$, one finds approximately (see Appendix)

$$\frac{1}{L} \int_{-\infty}^{+\infty} \frac{E_0^2(x,z)}{E_0^2(1)} dz = \frac{E_{0\ell}^2(x)}{E_0^2(1)} \frac{1}{2\Gamma} \ell n \left(\frac{e^{A_1(\theta+\tau)}}{e^{A_1(\theta+\tau)} - 1 + e^{-2\Gamma}} \right), \tag{30}$$

$$\frac{E_1^2(x,\tau = -L/2)}{E_0^2(1)} = \frac{E_{1\ell}^2(x)}{E_0^2(1)} \frac{1}{1 + e^{-A_1(\theta+\tau)} e^{-A_1 L} (-1 + e^{-2\Gamma})}, \tag{31}$$

where $\theta + \tau = a \int_1^x \left(\frac{v_{0z}}{v_{0x}} - \frac{v_{1z}}{v_{1x}} \right) dx'$, and $\Gamma = -(A_0 + A_1)L/2$ is the spatial growth factor. It should be noted that Eq. (30) is independent of the width of the propagation cone, and so is also, approximately, Eq.(31) since $(\theta + \tau) > L$.

In region I the electric fields are independent of z and there solutions are as found from a one-dimensional analysis [15]

$$\frac{E_0^2(x)}{E_0^2(1)} = \frac{E_{0\ell}^2(x)}{E_0^2(1)} \frac{1}{1 + p_r e^{(A_0 + A_1)(\theta + \tau)}} \tag{32}$$

$$\frac{E_1^2(x)}{E_0^2(1)} = \frac{E_{1\ell}^2(x)}{E_0^2(1)} \frac{1}{p_r + e^{-(A_0 + A_1)(\theta + \tau)}} \tag{33}$$

and satisfy $E_{0\ell}^2 + \frac{v_{1x}}{v_{0x}} E_{1\ell}^2 = E_0^2 + \frac{v_{1x}}{v_{0x}} E_1^2$. Then, if $E_0^2 \to 0$ one has $E_1^2 \to \frac{v_{0x}}{v_{1x}} E_{0\ell}^2(x) + E_{1\ell}^2(x)$, and the sideband will come out with all the pump power. On the other hand if the depletion of the pump occurs in region II, then the power density of the sideband can be much less than that of the pump. Complete depletion of the pump in region II occurs when $e^{-A_1(\theta + \tau)} = 0$. At that x, (30) and (31) give $E_0^2 = 0$ and $E_1^2 = E_{1\ell}^2$.

Let us now analize carefully Eq.(31). The sideband electric field E_1^2 gets larger when the denominator of Eq.(31) gets smaller, which happens when $e^{-2\Gamma} \ll 1$ and $e^{-A_1(\theta + \tau)} \sim 1$, (we note that $|A_1 L| \ll A_1(\theta + \tau)$ and that $e^{-A_1 L} \sim 1$). In order for $e^{-2\Gamma} \ll 1$, we need large growth factors (e.g. $\Gamma > 1$), that is either high densities, or low densities and large n_{1z}'s. At high densities or sufficiently high n_{1z}'s, we have $e^{-2\Gamma} \sim 0$, but we still need $e^{-A_1(\theta + \tau)} \sim 1$, i.e. $A_1(\theta + \tau) \sim 0$. Combining Eq.(28) with the definition of $(\theta + \tau)$, we get $A_1(\theta + \tau) \approx \frac{C E_{1\ell}^2 a (x - 1)}{v_{0x}}$, and thus, inside the plasma, $|x| < 1$, $A_1(\theta + \tau)$ will be small only if v_{0x} is sufficiently large. However as has already been pointed out, v_{0x} is always small and gets smaller as one increases the density. Hence no strong sideband fields are expected to be created in the main bulk of the plasma. The total rf-power is, of course, conserved, but it is now spread out in a larger region of space following the group velocity trajectory of the pump field (i.e. along $\tau = -L/2$). This power is introduced in the plasma through a two waveguide array, which for Alcator A has an area $h\,w = 20\ cm^2$; as the pump gets in the plasma the sideband it generates will be spread out in an area: $h\left(\frac{w}{2} + a \int_1^x \right.$

$\frac{v_{0z}}{v_{0x}}\,dx'$). For $ha = 76\ cm^2$, and $|\frac{v_{0z}}{v_{0x}}| > 30$, we find $ha \int_1^x \frac{v_{0z}}{v_{0x}}\,dx' > 2.3 \times 10^3\,(1-x)\ cm^2$. Thus, a strongly depleted pump does not lead necessarily to large amplitude sideband fields. The excitation of strong fields requires a strong interaction between the pump and the noise (say $\Gamma > 1$), and that this interaction is to occur near the mouth of the waveguides ($x \sim 1$). At the edge, x very close to 1, Γ is very large, larger than anywhere else; besides, Δx_w is also large and increases with decreasing density. Thus, at the edge the pump is just depleted in region I, and the one dimensional equations (32) and (33) are adequate to describe the depletion. The amplitudes of the excited fields will then be comparable to that of the launched pump field.

V. Nonlinear Theory, Calculations

A. The Plasma Edge

Let us now apply the nonlinear description of the previous section to Alcator A experiment, and let us start with the plasma edge. In Fig. 6, we are representing the averaged square pump electric field, as given by Eq. (30), for the minimum depletion distance out of the resonance cone, $\Delta x_w = \frac{w/a}{|v_{0z}/v_{0x} - v_{1z}/v_{1x}|}$, as a function of the sideband frequency spectrum. We take the rf-power to be 32 Kw and according to the linear theory, $n_{0z} = 3$. In the case of low density, Fig. 6A, we see that the wave-numbers $n_{1z} = 6$ and 8, deplete most of the pump power. For the high density case, Fig. 6B, the wave-numbers, $n_{1z} = 1.5$ and 4 are already able to essentially deplete the pump. Let us call n_{zth} the minimum n_{1z} for which the pump suffers an appreciable depletion in the distance Δx_w. This threshold will become smaller, and eventually equal to 1, as the density increases. When the density is very small one has $n_{zth} \gg 1$. In our two examples one can approximately fix $n_{zth} \sim 7$, for the low density regime, $n_{zth} \sim 3$, for the high density regime.

For strong excitation of large amplitude sideband fields we require that pump depletion is to occur mainly in region I, that is in a distance from the edge approximately equal to Δx_w. This characteristic distance, Δx_w, is a function of density and sideband frequency ω_1. At the edge ω_1 is so close to ω_0 and the density is so small that Δx_w is usually large. For example in Fig. 6, and for those ω_1 that give the strongest depletion we find, for the low density regime $\Delta x_w \sim 0.07$, and for the high density regime $\Delta x_w \sim 0.04$, (to recover Δx_w in real magnitude one has to multiply the above dimensionless numbers by the minor radius of the tokamak, $a = 10\ cm$). The large amplitude excited fields, $n_{1z} \geq n_{zth}$, will propagate in a cone of width equal to the pump width, $L \sim 2.5\ cm$. In terms of wave-numbers this means that the width of the excited spectrum is of the order of the width of the pump spectrum, $\Delta n_{1z} \sim 4$ (in general one has $\Delta n_{1z} \leq \Delta n_{0z} \sim 4$). The question that arises now is for $n_{1z} \geq n_{zth}$, which are the selected n_z's that deplete the pump. We are not going to carry out in the present paper the calculations that lead to the excited spectrum. As a general

criterion, we take those $n_{1z} \geq n_{zth}$ that "deplete first" (i.e. those with the larger group velocities) as the ones that deplete the pump. In order to support this criterion, let us present some physical arguments on what would happen if the excited fields have the largest possible n_{1z}'s. Initially the pump spectrum is centered around the value $n_{0z} \sim 3$; after decaying, the excited spectrum will be centered at, say $n_{1z} \sim 45$. Let us consider the excited spectrum as a new pump which essentially differs from the initial pump in the wave-number spectrum. This new pump, centered at $n_{0z} \sim 45$, may decay again. The spatial growth factor increases linearly with n_{0z}, see Eq. (4); this means that Γ is multiplied by a factor of 15 with respect to the values it took when n_{0z} was 3, which makes this new pump highly unstable. This would initiate a quick cascade evolution toward smaller n_z's until the pump reaches the most stable parametric decay, i.e. near the lowest n_{1z} for which the pump completely depletes, which will be what we call the threshold n_{zth}. We note that if the highest possible n_{1z}'s are excited, they could damp a certain amount of the rf-power on the electrons before the new pump is able to penetrate inside the plasma. Nevertheless, in order to achieve a very high excited new pump (i.e. $n_{1z} > 45$) one needs to decrease drastically the density of the plasma, since otherwise the rate of decay toward smaller n_z's will be always larger than the linear Landau-damping rate, and thus the cascading processes toward smaller n_z's will dominate.

It should be noted that n_{zth} and the pump spectrum penetrating in the plasma, depend on the assumed noise level. The thermal noise level is too small, and nonlinear processes always enhances it. The experimental data show that for $n_0 = 1.5 \times 10^{14}\ cm^{-3}$, the electrons are heated close to the center of the plasma. For this to occur, we require the excitation of the wave-numbers, $n_{1z} = 6$ and 7, which in turn leads to the estimation $A_1/A_0 = 5 \times 10^{-4}$ so that appreciable pump depletion should occur into these wave-numbers. We want to remark that it is beyond the scope of this paper to present quantitative results on the stability of the excited spectrum; with arguments as the ones presented in this section, we only attempt to present a qualitative picture of the evolution for these quasimode excitations and mainly wish to point out how they scale in the different regimes of plasma parameters.

Now, we can summarize the situation at the plasma edge as follows. The pump is

completely depleted in this region, and the excited spectrum has a frequency very close to the initial pump frequency and propagates in a cone of width approximately equal to the waveguides width. However, the wave-number spectrum may be very different from the initial linear spectrum. For $n_0 = 1.5 \times 10^{14}\ cm^{-3}$, $5 < n_{1z} < 10$, and for $n_0 = 5 \times 10^{14}\ cm^{-3}$, $1 < n_{1z} < 6$. The excited spectrum will act as a new pump inside the plasma, which is now centered at about $n_{0z} \sim 7$, for the low density regime, and around $n_{0z} \sim 3$, for the high density regime. We note that by decreasing the density, n_{0z} will become larger, and all the rf-power may be modeconverted or damped on the electrons, before getting in the main bulk of the plasma.

B. Inside the Plasma

The excited spectrum at the plasma edge will act as a new pump inside the plasma, centered at n_{0z} = 7 and n_{0z} = 3, for the low and high density regimes, respectively. We assume that 40% of the rf-power will remain close to the edge and never be able to act in the plasma. This may occur because the pump can excite, close to the plasma edge, new waves of higher n_z 's (e.g. n_{1z} > 12, for the low density regime, and n_{1z} > 5 for the high density regime). The part of the power which goes into these high n_{1z} 's will be either modeconverted or transfered to the electrons via Landau-damping, before the new pump penetrates well inside the plasma. Under this assumption,the amount of power penetrating into the plasma in a resonance cone is, for both regimes, about 17.5 Kw.

The essential difference between the main bulk of the plasma and the plasma edge is the rapid rise in the electron temperature, which is faster than the corresponding rise in density. We have already seen that the growth factors are here smaller than at the plasma edge. Consequently, pump depletion is expected to be weaker, and occur in a distance, Δx_d, much larger than Δx_w. The excitation of sideband fields will occur mostly in region II, and their amplitudes will be much smaller than that of the launched pump electric field. The way in which the excited spectrum will be selected is also different from the plasma edge. First of all, the range of variation for n_{1z} is now more restricted by the increasing electron temperature and by the increasing plasma density. The largest possible n_{1z} 's (e.g. $n_{1z} \sim 12$ for the low density regime and $n_{1z} \sim 5$ for the high density regime) will interact with the new pump first because they have the largest growth factors, and will deplete a large amount of the rf-power before the new pump is able to get well inside the plasma. However, their growth rates are now only moderate and because of that we assume that cascading to lower n_z 's does not take place. Thus, the part of the power that is transfered to the largest possible n_{1z} 's, will be either modeconverted into thermal modes or Landau-damped on the electrons. The amount of rf-power transfered to the highest n_{1z} 's increases by increasing the central peak density. For the high density regime we find that the new pump is completely depleted close to the plasma

limiter. In the low density regime the depletion is not so complete and there may be still an appreciable amount of power getting into the plasma.

To illustrate the above comments, let us present some calculations, first for the low density regime. The nonlinear power spectrum is assumed centered at $n_{0z} \sim 7$; we remind that Γ increases with increasing n_{0z}, so the depletion is stronger for the nonlinearly generated spectrum than it would be for the original linear one (i.e. $n_{0z} \sim 3.5$). In Fig. 7, we are representing with continuous lines the square pump field averaged along the resonance cone, as given in Eq.(30), and with dotted lines the evolution of the rf-power, averaged also in the pump cone and normalized to the initial rf-power of 17.5 Kw. The pump electric field suffers simultaneously the effect of the depletion, due to the parametric procceses, and a spatial enhancement due to the inhomogenities of the plasma. When the depletion is small the pump electric field will grow with x until the depletion overcomes this growth, and makes E_0^2 decrease down to zero. We take n_{1z} = 2 and 5 in Fig. 7A, and n_{1z} = 12 in Fig. 7B. We also take one of the maximum growing frequencies ω_1/ω_0= 0.86 (Fig. 7A) and ω_1/ω_0= 0.9 (Fig. 7B) and for these ω_1's, we find Δx_w = 0.01 and 0.015, respectively. For n_{1z} = 2, the depletion is neglegible; for n_{1z} = 5 pump depletion starts at $x \sim 0.5$ and the overall depletion is around 35%. In Fig. 7B, x goes only up to 0.5, and this is due to modeconversion of the excited sideband electric field of wave-number n_{1z} = 12 and frequency ω_1/ω_0= 0.9. However, this excited field starts transfering energy to the electrons at about x = 0.75, before modeconversion into thermal modes takes place. Thus, an appreciable amount of the available rf-power, say 40%, may be damped on the electrons and heats the plasma close to the plasma limiter. Besides, this will reduce the amount of power penetrating into the plasma center. The part of the power that penetrates may excite lower wave-numbers, such as n_{1z} = 5, close to the plasma center. However, to properly calculate how much power goes into the smallest n_{1z}'s one should make a more careful analysis than the one presented here, and substract from the total power that part that has already gone into the excitation of the highest n_{1z}'s.

In Fig. 8 we study, for the low density regime, how the excited sideband electric field evolves in x (continuous lines) compared to the linear evolution of the noise electric field (dotted

lines), as given in Eqs.(29) and (31), for n_{1z} = 5, ω_1/ω_0 = 0.86 (Fig. 8A) and n_{1z} = 12, ω_1/ω_0 = 0.9 (Fig. 8B). We see that the amplitude of the excited fields are never comparable to the amplitude of the launched pump field. This, as explained in the last section, is due to the fact that the pump is moving parallel to the magnetic field. Thus, a pump depleted in a distance, Δx_d, in x of the order of 2 or 3 *cm* has traveled a much larger distance in the z-direction, along which the power is continuosly spread out. It should be noted that the sideband fields created close to the plasma edge, as in Fig. 8B, are always larger than the ones created well inside the plasma, as in Fig. 8A. This is due to the fact that v_{0x} is larger when the density decreases, and about the same amount of power will be put in a smaller distance following the pump trajectory. The ripple in Fig. 8A at $x \sim 0.7$, is due to the fact that pump and sideband are ocasionally uncoupled because of the spatial inhomogenities of the toroidal magnetic field.

Next, we shall present some nonlinear calculations for the high density regime. In Fig. 9 we study how the pump is depleted in x, for two different values of n_{1z}, n_{1z} = 2 (Fig. 9A) and n_{1z} = 5 (Fig. 9B). The pump power spectrum is centered at $n_{0z} \sim 3$, the available power is in both examples, 17.5 *Kw*, and the frequency of the excited fields is the same in both cases, ω_1/ω_0 = 0.95. For this ω_1 we find that $\Delta x_\omega \sim 0.015$, and the distance in which the pump is depleted is of the order of 2 or 3 *cms*. We see that for n_{1z} = 2, (Fig. 9A), pump depletion starts at $x \sim 0.7$. For n_{1z} = 5 (Fig. 9B), the depletion starts at $x \sim 0.9$, and the pump is effectively depleted (there is only a 10% left) at $x \sim 0.6$. Thus, the smallest n_{1z} 's will not deplete the pump, since the highest n_{1z} 's will interact sooner and do it first. The reason why in Fig. 9A, x goes only from 1 to 0.3, is due to modeconversion of the pump electric field centered at n_{0z} = 3.5. From x = 0.3 to 0, one should take into account only that part of the spectrum, if any, in between n_{0z} = 2 and 3 (that is a centered spectrum at n_{0z} = 2.5). In Fig. 9B, x varies from 1 to 0.5, but the reason is now modeconversion of the excited sideband electric field whose frequency and wave-number are respectively ω_1 = 0.95 ω_0 and n_{1z} = 5. This effect of modeconversion of the excited spectrum is having crucial consequences, since all the rf-power will be transfered to the highest n_{1z} 's and modeconverted into thermal modes, before reaching the plasma center. A cut-off in the amount of rf-power getting into the

plasma center is thus predicted for sufficiently high densities. In Fig. 10, we are showing the excited fields for n_{1z} = 2 (Fig. 10A), n_{1z} = 5 (Fig. 10B), and ω_1/ω_0 = 0.95. We observe again that their amplitudes (continuous lines) are very small compared to the initial pump amplitude, but considerably much larger than the amplitude of the electric noise (dotted lines). We also note that fields excited closer to the plasma edge (Fig. 10B) have larger amplitudes than those excited near the plasma center (Fig. 10A).

VI. Summary and Discussion

Parametric excitations of the quasimode type present different characteristics in two distinct region of a tokamak plasma, the plasma edge and the main bulk of the plasma. They also lead to different results when considering the two regimes of low and high densities, which are represented respectively by the peak in densities: $n_0 = 1.5 \times 10^{14} cm^{-3}$ and $5 \times 10^{14} cm^{-3}$.

At the edge of the plasma, we have found that parameric excitations are very strong and that, in fact, the pump is depleted in this region. The excited spectrum has a frequency very close to the initial pump frequency, while the wave-number spectrum may be very different from the initial linear spectrum (i.e. $1 \leq n_{0z} \leq 5$). As the temperature is very low here, the excited spectrum can, in principle, run from $n_{1z} = 1$ to say $n_{1z} = 50$. The spatial growth factor increases linearly with n_{1z}. Besides, and through the nonlinear theory, we have argued that there exist a certain threshold, that we call n_{zth}, such that for $n_{1z} \geq n_{zth}$, the pump will be essentially depleted. We have not calculated the detailed excited spectrum, and as a criterion, we have been taken those $n_{1z} \geq n_{zth}$ which "deplete first" (i.e. those which have the larger group velocities) as the ones that deplete the pump. Due to the finite spatial extension of the pump, the excited fields have a maximum extension in wave-numbers, $\Delta n_{1z} \sim 4$ or 5. By passing from the high density regime to the low one, n_{zth} becomes larger and eventually, by decreasing sufficiently the density, n_{zth} can be large enough so that the excited spectrum is modeconverted into thermal modes or Landau-damped on the electrons, as soon as it gets into the plasma. For sufficiently high densities, and following the above criterion, the excited spectrum will be similar in wave-numbers to the initial linear spectrum. In order to support this criterion, we have presented the following argument: Let us assume that the pump decays into the highest possible n_{1z} 's, and let us consider the excited spectrum as a new pump, centered at say $n_{0z} \sim 45$, which may decay again. The spatial growth factor Γ increases linearly with n_{0z} and n_{1z}. This means that Γ is multiplied by a factor of 15 with respect to the values it took when n_{0z} was 3. This new pump is now highly unstable to quasimode parametric decay, and it will quickly cascade toward smaller n_{1z} 's to become more stable. This process will be

stopped when the new n_z and Γ are sufficiently small, so that the excited sideband spectrum cannot further decay. Thus, the most stable parametric decay is in general, well represented by the value n_{zth}. The highest n_{1z} excited spectra can be reached just by decreasing sufficiently the density of the plasma. It should be noted that if the excited fields have large n_z 's (e.g. $n_z \sim 50$) they can transfer part of their energy to the electrons via Landau-damping. However, this can only happen for very low densities, since for sufficiently high densities the rate of decaying into smaller n_z 's, is always very large and, in fact, it is larger than the linear damping rates. Then a cascading proccess toward smaller n_z 's would dominate, and the energy will not be transfered to the particles at the edge.

As one gets inside the plasma, the plasma parameters will change: the density will increase and so will the temperatures; the increase in the temperatures being much faster than the corresponding one in density. This will also change the characteristics of the excited spectrum. Thus, the most likely parametric excitations will be different, in terms of wave-numbers, frequency, and power density, from the ones found at the edge. We start with the nonlinear spectrum excited at the plasma edge. The frequency is just the same as the initial pump freqency. The power density, or otherwise the width of the excited sideband cone, is not different from the initial one, at the mouth of the waveguides. But the wave-number spectrum differs from the linear spectrum: for the low density regime, it is centered at $n_{0z} \sim 7$, and for the high density regime, it is centered at about $n_{0z} \sim 3$. Notice that we are already considering the excited spectrum as a new pump, which may decay into new n_z 's as it propagates in the plasma. The possible n_{1z} 's that can be excited in the plasma are not as large as they were at the plasma edge (say, $n_{1z} \leq 12$, for the low density case, and $n_{1z} \leq 6$, for the high density case). The spatial growth factors are usually smaller than the ones found at the plasma edge due to the rapid rise in the electron temperatue. In the low density regime, a large amount of the available rf-power may decay into the highest n_{1z} 's, as say $n_{1z} = 12$, before reaching the plasma center . This part of the power will be transfered to the electrons, via Landau-damping, and never reach the plasma center. In the high density regime further decays into new wave-numbers will also occur as soon as the new pump penetrates into the plasma .

The rf-power will be completely transfered to the larger n_{1z} 's, such as n_{1z} = 5, and modeconverted into thermal modes before it is able to reach the plasma center. The lowest wave-numbers, such as n_{1z} = 2, may be excited close to the plasma center, but by then only a fraction of the power, or very little, may be left.

The excited spectrum presents inside the plasma the following characteristics: The frequency is usually smaller than the pump frequency, and becomes closer to it with increasing density. The power density is much lower than the original one, at the waveguides mouth, and has spread to many other wave-numbers. Thus, the rf-power will no longer be confined to propagate in a well defined resonance cone, but will be dispersed across the plasma cross section.

Appendix

The function $S(\theta) - T(\tau)$ is given in terms of A_1 and $A_0(z)$ ($A_0(z) = A_0$ if $|z| \le L/2$ and $A_0(z) = 0$ if $|z| > L/2$), by means of the following equation,

$$S(\theta) - T(\tau) = 1 + \int_0^{\theta} dy A_1 exp\left(\int_0^{y} (A_0 + A_1)dz\right) + \int_0^{-\tau} dy A_0 exp\left(\int_0^{y} (A_0 + A_1)dz\right) \quad (A.1)$$

In region II ($|\tau| \le L/2$, $\theta < -L/2$), one finds:

$$S(\theta) - T(\tau) = \frac{1}{(A_0 + A_1)} \{-A_0 e^{-(A_0+A_1)L/2} + (A_0 + A_1) e^{-A_0 L/2} e^{A_1\theta} + A_0 e^{-(A_0+A_1)\tau}\} \quad (A.2)$$

and through Eqs. (25) and (26),

$$\psi_0 = \frac{A_0(A_0 + A_1)}{(A_0 + A_1) e^{A_1(\theta+\tau)} e^{A_0(\tau - L/2)} - A_0 e^{(A_0+A_1)(\tau - L/2)} + A_0} \quad (A.3)$$

$$\psi_1 = \frac{A_1(A_0 + A_1)}{(A_0 + A_1) - A_0 e^{-A_1(\theta+L/2)} + A_0 e^{-A_1(\theta+\tau)} e^{-A_0(\tau - L/2)}} , \quad (A.4)$$

From Eq. (A.4), taking $\tau = -L/2$ and contemplating the definitions, Eqs. (27), (28) and (29), it is easy to recover the form of Eq. (31). In order to derive Eq. (30), let us consider that $A_1(\tau - L/2) < A_0(\tau - L/2)$ since $p_\tau = \frac{A_1}{A_0} = 5 \times 10^{-4}$, and that $A_1(\tau - L/2) < A_1(\theta + \tau)$ since $\theta < -L/2$. These estimations allow us to write,

$$\psi_0 = \frac{(A_0 + A_1)}{e^{A_0(\tau - L/2)}[-1 + (1 + p_\tau) e^{A_1(\theta+\tau)}] + 1} , \quad (A.5)$$

where now the only z-dependencies come from $z_\tau \equiv -(\tau - L/2) = z - a\int_1^{x} \frac{v_{0z}}{v_{0x}} + L/2$. Eq. (A.5) can be integrated exactly with respect to z_τ from $z_\tau = 0$ to $z_\tau = L$, and the result is just Eq. (30).

Acknowledgements

We are grateful to Dr. A. Sen for many helpful discussions, and to Dr. J. L. Kulp for computational help. One of us (E. V) has been supported by grant PFPI (MEC) Spain. This work has been supported by the U.S. Department of Energy Contract (ET78-S-02-4682).

References

1. Schuss, J. J., Fairfax, S., Kusse, B., Parker, R.R., Porkolab, M., et al, Lower Hybrid Wave Heating in the Alcator A Tokamak, Massachusetts Institute of Technology. Plasma Fusion Center Rep. JA-79-4

2. Bernabei, S., Daugnney, C., Hooke, W., Motley, R., Nagashima, T., et al, in Third Symposium on Plasma Heating in Toroidal Devices, Editrice Compositore-Bologna, Italy, (1976) 68.

Porkolab, M., Bernabei, S., Hooke, W. M., Motley, R. W., Nagashima, T., Phys. Rev. Lett. 38 (1977) 230.

Gormezano, C., Blanc, P., Durvaux, M., Hess, W., Ichtchenko, G., et al, in Third Topical Conference on Radio Frequency Plasma Heating, California Institute of Technology, Pasadena, California, U.S.A., (1978) A3-1.

Nagashima, T., Fujisawa, N., in Heating in Toroidal Plasmas (Proc. joint Varenna-Grenoble Int. Symp. Grenoble, 1978) Vol. 2, Grenoble, France, (1978) 281.

Briand, P., Dupas, L., Golovato, S. N., Singh, C. M., Melin, G., et al, in Heating in Toroidal Plasmas (Proc. joint Varenna-Grenoble Int. Symp. Grenoble, 1978) Vol. 2, Grenoble, France, (1978) 455.

Singh, C. M., Briand, P., Dupas, L., Golovato, S. N., Grelot, P., in Heating in Toroidal Plasmas (Proc. joint Varenna-Grenoble Int. Symp. Grenoble, 1978) Vol. 2, Grenoble, France, (1978) 457.

Lohr, J., Chan, V. S., Luxon, J. L., Moeller, C. P., Ohkawa, T., et al., Bull. Am. Phys. Soc. 23 (1978) 821.

3. Porkolab, M., Phys. Fluids 17 (1974) 1432.

4. Wersinger, J. M., Kritz, A. H., Troyon, F., Weibel, E. S., in Third International Meeting on Theoretical and Experimental Aspects of Heating of Toroidal Plasmas, Commissariat a L'Energie Atomique, Grenoble, France (1976) 161.

Porkolab, M., Phys. Fluids 20 (1977) 2058.

Sperling, J. L., Chu, C., Aspects of Nonlinear Heating by Lower Hybrid Waves, General Atomic Company Rep. GA-A14537 (1977).

Tripathi, V. K., Liu, C. S., Grebogi, C., Phys. Fluids 22 (1979) 301.

5. Berger, R. L., Chen, L., Kaw, P. K., Perkins, F. W., Phys. Fluids 20 (1977) 1864.

6. Chen, L., Berger, R. L., Nucl. Fusion 17 (1977) 779.

7. Sen, A., Karney, C. F. F., Bers, A., Phys. Fluids 21 (1978) 861.

8. Rogister, A., Phys. Rev. Lett. 34 (1975) 80.

Rogister, A., Hasselberg, G., Phys. Fluids 19 (1976) 108.

Hasegawa, A., Chen, L., Phys. Fluids 18 (1975) 1321.

Berger, R. L., Chen, L., Perkins, F. W., Princenton Plasma Physics Laboratory Report PPPL-1307 (1976).

9. Scaturro, L. S., Kusse, B., Nucl. Fusion 18 (1978) 1717.

10. Ichimaru, S., Basic Principles of Plasma Physics (a Statistical Approach), W.A. Benjamin, Inc., London (1973).

11. Bers, A., in Third Topical Conference on Radio Frequency Plasma Heating, California

Institute of Technology, California (1978) A 1.

12. Apgar, E., Coppi, B., Gondhalekar, A., Helava, H., Komm, D., et al. , in Plasma Physics and Controlled Nuclear Fusion Research (Proc. 6th Int. Conf. West Germany, 1976) Vol.1,. IAEA, Vienna (1977) 247.

13. Brambilla, M., Nucl. Fusion 16 (1976) 47.

14. Krapchev, V., Bers, A., Nucl. Fusion 18 (1978) 519.

15. Chu, F. Y. F., Karney, C. F. F., Phys. Fluids 20 (1977) 1728.

Figure Captions

Figure 1. Linear pump propagation cone and sideband group velocity trajectory.

Figure 2A. Modeconversion of the pump electric field at different x 's for different n_z 's. $n_0 = 1.5 \times 10^{14}\ cm^{-3}$.

Figure 2B. Modeconversion of the pump electric field at different x 's for different n_z 's. $n_0 = 5 \times 10^{14}\ cm^{-3}$.

Figure 3A. Inside the Plasma. Spatial growth factor vs. sideband frequency spectrum. $n_0 = 1.5 \times 10^{14}\ cm^{-3}$, $n_{0z} = 3.5$, $n_{1z} = 2$, $P_0 = 17.5\ Kw$.

Figure 3B. Inside the Plasma. Spatial growth factor vs. sideband frequency spectrum. $n_0 = 5 \times 10^{14}\ cm^{-3}$, $n_{1z} = 2$. We take at $x = 0.75$, $n_{0z} = 3.5$ with $P_0 = 17.5\ Kw$, and at $x = 0.25$, $n_{0z} = 2.5$ with $P_0 = 7.5\ Kw$.

Figure 3C. Inside the Plasma. Spatial growth factor vs. sideband frequency s pectrum. $n_0 = 1.5 \times 10^{14}\ cm^{-3}$, $n_{0z} = 3.5$, $n_{1z} = 5$, $P_0 = 17.5\ Kw$.

Figure 3D. Inside the Plasma. Spatial growth factor vs. sideband frequency spectrum. $n_0 = 5 \times 10^{14}\ cm^{-3}$, $n_{0z} = 3.5$, $n_{1z} = 5$, $P_0 = 17.5\ Kw$.

Figure 4. Inside the Plasma. Spatial growth factor vs. sideband frequency spectrum. $n_0 = 1.5 \times 10^{14}\ cm^{-3}$, $n_{0z} = 6.5$, $n_{1z} = 12$, $P_0 = 17.5\ Kw$.

Figure 5A. Plasma Edge. Spatial growth factor vs. sideband frequency spectrum. $n_0 = 1.5 \times 10^{14}\ cm^{-3}$, $n_{0z} = 3$, $P_0 = 32\ Kw$.

Figure 5B. Plasma Edge. Spatial growth factor vs. sideband frequency spectrum. $n_0 = 5 \times 10^{14}\ cm^{-3}$, $n_{0z} = 3$, $P_0 = 32\ Kw$.

Figure 6A. Plasma Edge. Nonlinear depletion of the square of the pump electric field vs. sideband frequency spectrum at the fixed position from the edge, Δx_w. $n_0 = 1.5 \times 10^{14}\ cm^{-3}$, $n_{0z} = 3$, $P_0 = 32\ Kw$.

Figure 6B. Plasma Edge. Nonlinear depletion of the square of the pump electric field vs. sideband frequency spectrum at the fixed position from the edge, Δx_w. $n_0 = 5 \times 10^{14}\ cm^{-3}$, $n_{0z} = 3$, $P_0 = 32\ Kw$.

Figure 7A. Inside the Plasma. Nonlinear evolution of the square of the pump electric field and of the pump power density vs. plasma position. $n_0 = 1.5 \times 10^{14}\ cm^{-3}$, $n_{0z} = 6.5$, $\frac{\omega_1}{\omega_0} = 0.86$, $P_0 = 17.5\ Kw$.

Figure 7B. Inside the Plasma. Nonlinear evolution of the square of the pump electric field and of the pump power density vs. plasma position. $n_0 = 1.5 \times 10^{14}\ cm^{-3}$, $n_{0z} = 6.5$, $n_{1z} = 12$, $\frac{\omega_1}{\omega_0} = 0.9$, $P_0 = 17.5\ Kw$.

Figure 8A. Inside the Plasma. Nonlinear evolution of the square of the excited sideband electric field and linear evolution of the electric noise vs. plasma position. $n_0 = 1.5 \times 10^{14}\ cm^{-3}$, $n_{0z} = 6.5$, $n_{1z} = 5$, $\frac{\omega_1}{\omega_0} = 0.86$, $P_0 = 17.5\ Kw$.

Figure 8B. Inside the Plasma. Nonlinear evolution of the square of the excited sideband electric field and linear evolution of the electric noise vs. plasma position. $n_0 = 1.5 \times 10^{14}\ cm^{-3}$, $n_{0z} = 6.5$, $n_{1z} = 12$, $\frac{\omega_1}{\omega_0} = 0.9$, $P_0 = 17.5\ Kw$.

Figure 9A. Inside the Plasma. Nonlinear evolution of the square of the pump electric field and of the pump power density vs. plasma position. $n_0 = 5 \times 10^{14}\ cm^{-3}$, $n_{0z} = 3.5$, $n_{1z} = 2$, $\frac{\omega_1}{\omega_0} = 0.95$, $P_0 = 17.5\ Kw$

Figure 9B. Inside the Plasma. Nonlinear evolution of the square of the pump electric field and of the pump power density vs. plasma position. $n_0 = 5 \times 10^{14}\ cm^{-3}$, $n_{0z} = 3.5$, $n_{1z} = 5$, $\frac{\omega_1}{\omega_0} = 0.95$, $P_0 = 17.5\ Kw$.

Figure 10A. Inside the Plasma. Nonlinear evolution of the square of the excited sideband electric field and linear evolution of the electric noise vs. plasma position. $n_0 = 5 \times 10^{14}\ cm^{-3}$, $n_{0z} = 3.5$, $n_{1z} = 2$, $\frac{\omega_1}{\omega_0} = 0.95$, $P_0 = 17.5\ Kw$.

Figure 10B. Inside the Plasma. Nonlinear evolution of the square of the excited sideband electric field and linear evolution of the electric noise vs. plasma position. $n_0 = 5 \times 10^{14}\ cm^{-3}$, $n_{0z} = 3.5$, $n_{1z} = 5$, $\frac{\omega_1}{\omega_0} = 0.95$, $P_0 = 17.5\ Kw$.

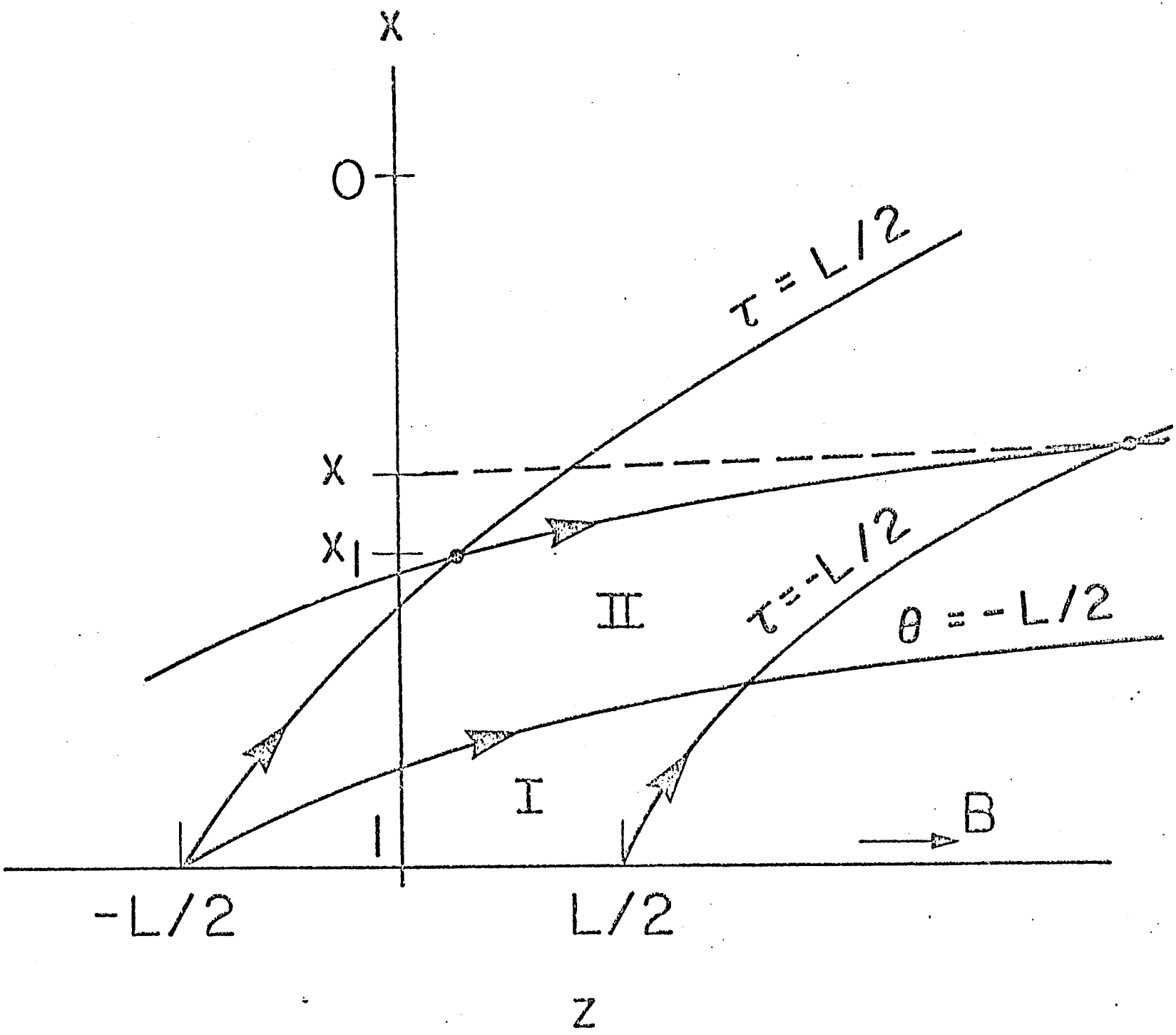

FIGURE 1

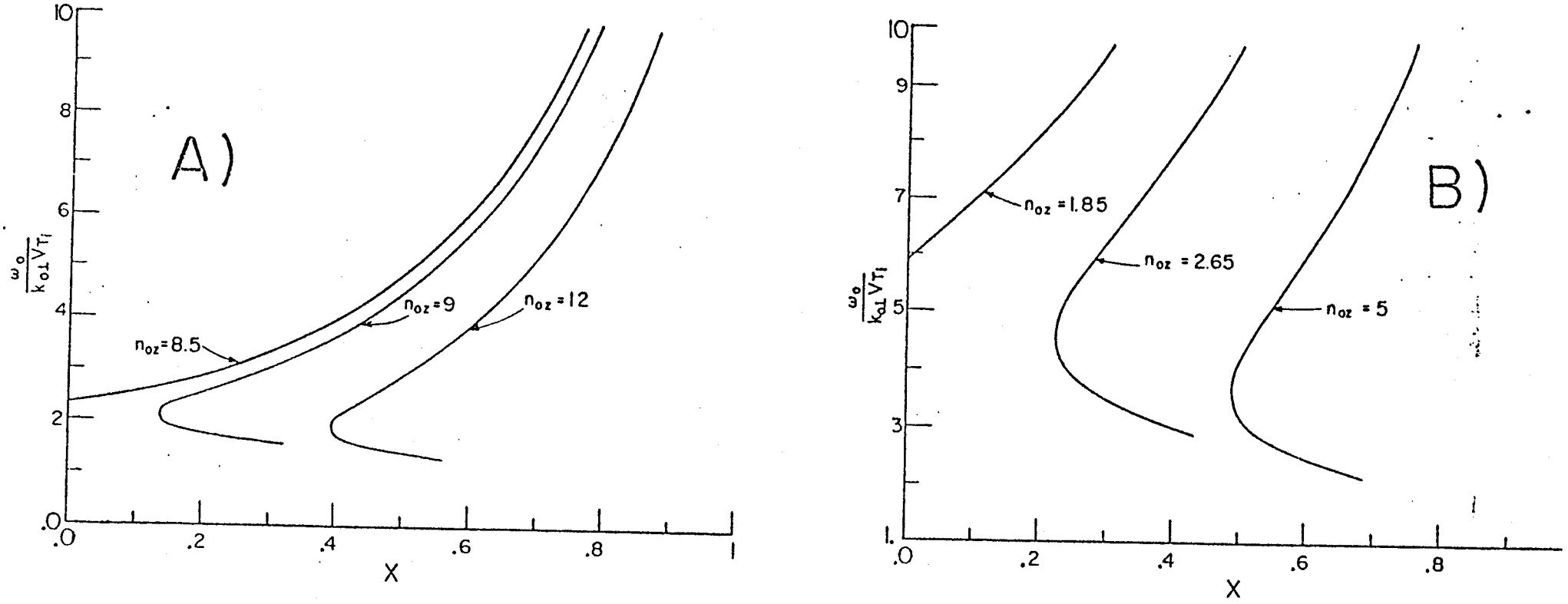
A)
B)
$\frac{\omega_o}{k_{o\perp} V_{Ti}}$
X
n_{oz}=8.5
n_{oz}=9
n_{oz}=12
n_{oz}=1.85
n_{oz}=2.65
n_{oz}=5
0
.2
.4
.6
.8
1
2
3
4
5
6
7
8
9
10

FIGURE 2

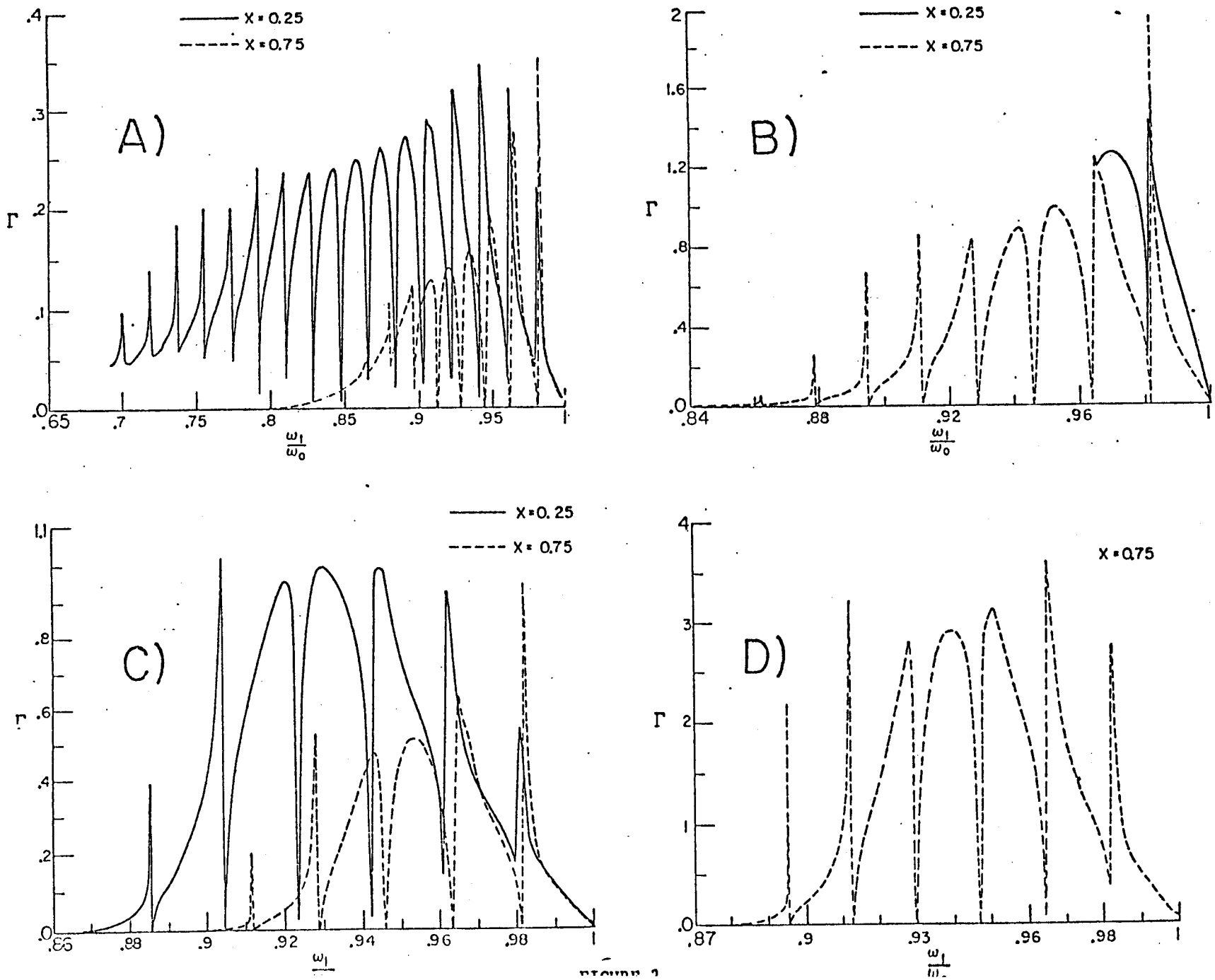
A)
X = 0.25
X = 0.75
Γ
.4
.3
.2
.1
0
.65
.7
.75
.8
.85
.9
.95
1
ω1/ω0
B)
X = 0.25
X = 0.75
Γ
2
1.6
1.2
.8
.4
0
.84
.88
.92
.96
1
ω1/ω0
C)
X = 0.25
X = 0.75
Γ
1.1
.8
.6
.4
.2
0
.86
.88
.9
.92
.94
.96
.98
1
ω1
D)
X = 0.75
Γ
4
3
2
1
0
.87
.9
.93
.96
.98
1
ω1

FIGURE 1

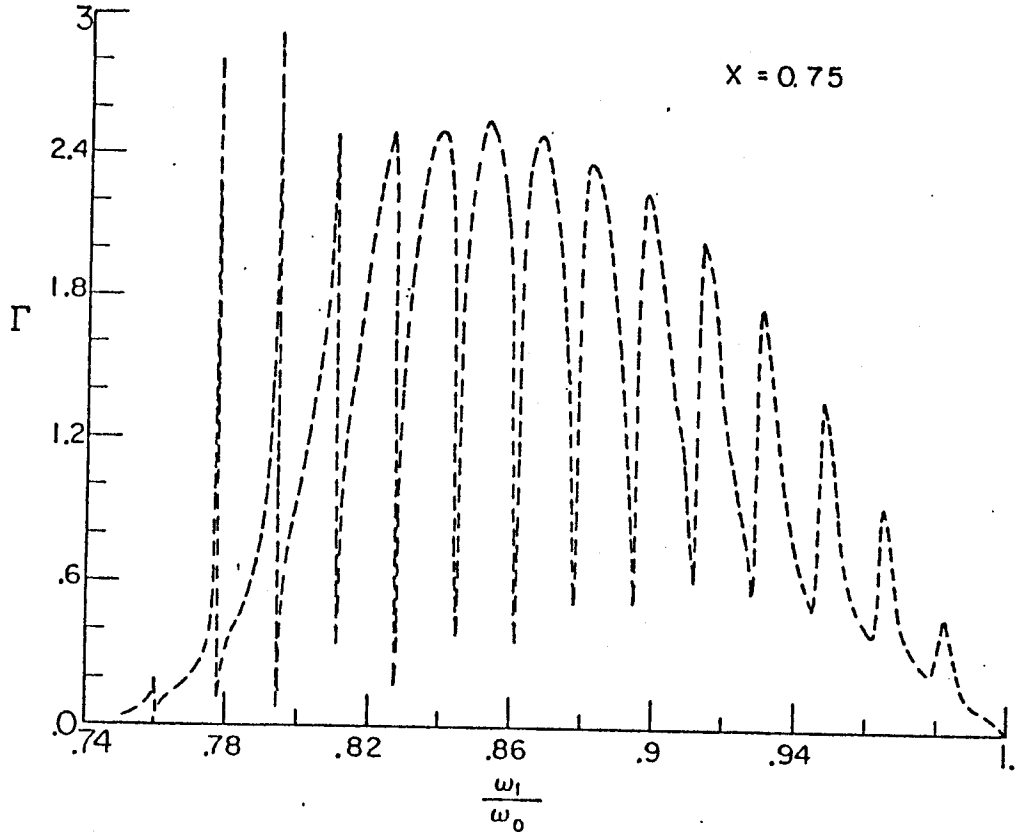

FIGURE 4

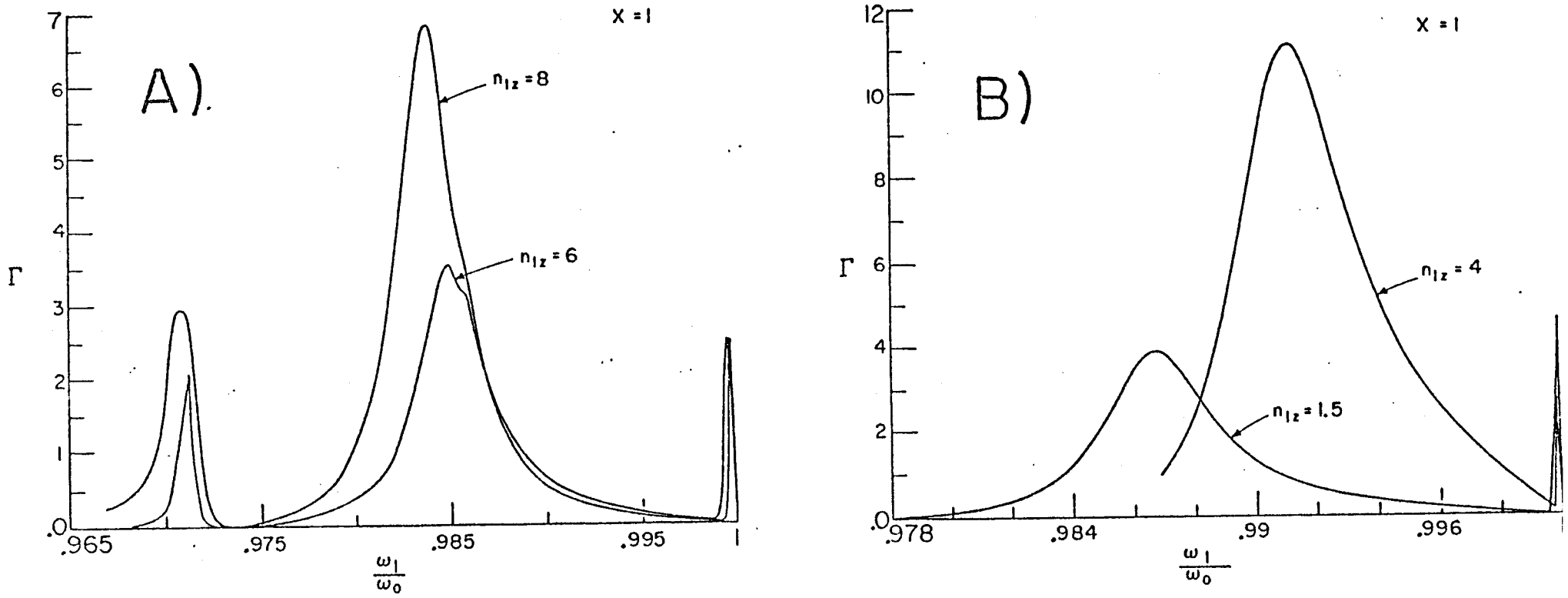
A).
X = 1
$n_{1z} = 8$
$n_{1z} = 6$
Γ
7
6
5
4
3
2
1
.0
.965
.975
.985
.995
1
$\frac{\omega_1}{\omega_0}$
B)
X = 1
$n_{1z} = 4$
$n_{1z} = 1.5$
Γ
12
10
8
6
4
2
.0
.978
.984
.99
.996
$\frac{\omega_1}{\omega_0}$

FIGURE 5

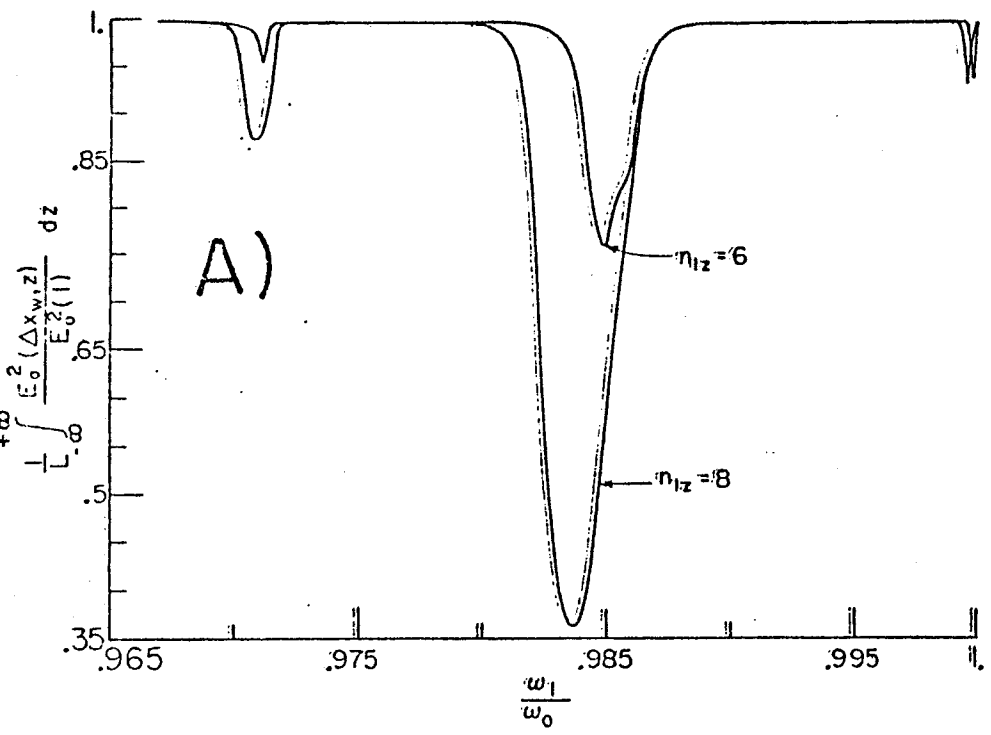
A)
$n_{1z} = .6$
$n_{1z} = .8$
1.
.85
.65
.5
.35
.965
.975
.985
.995
1.
$\frac{\omega_1}{\omega_0}$
$\frac{1}{L}\int_{-8}^{+8} \frac{E_o^2(\Delta x_w, z)}{E_o^2(1)}\, dz$

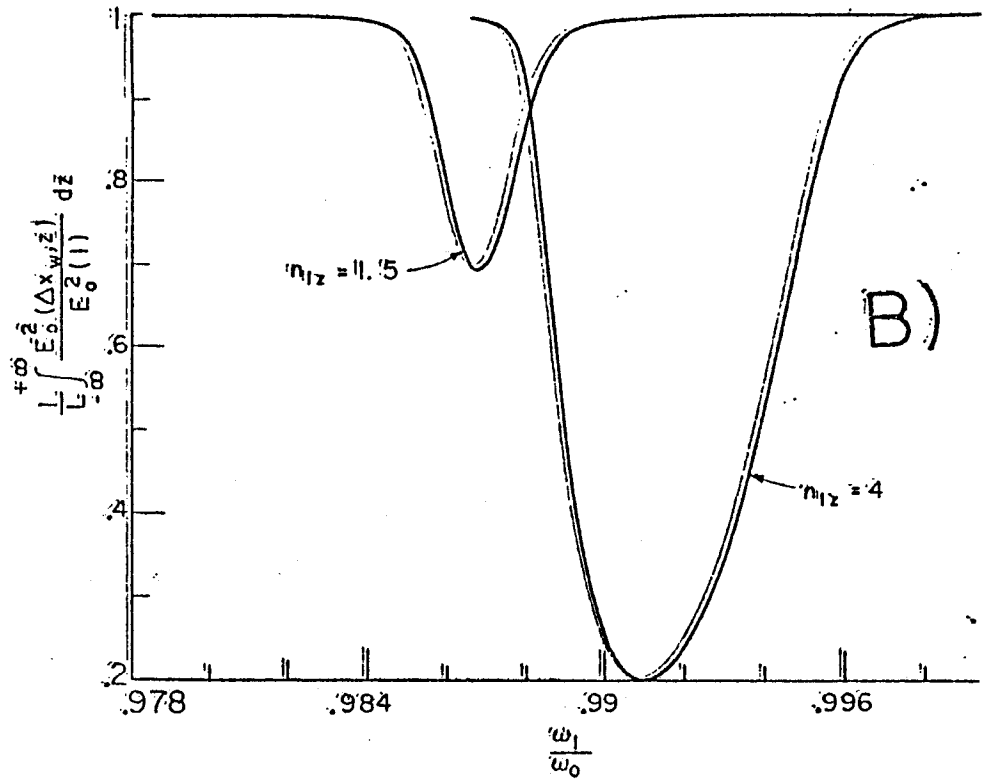
B)
$n_{1z} = 1.5$
$n_{1z} = .4$
1.
.8
.6
.4
.2
.978
.984
.99
.996
$\frac{\omega_1}{\omega_0}$
$\frac{1}{L}\int_{-8}^{+8} \frac{E_o^2(\Delta x_w, z)}{E_o^2(1)}\, dz$

FIGURE 6

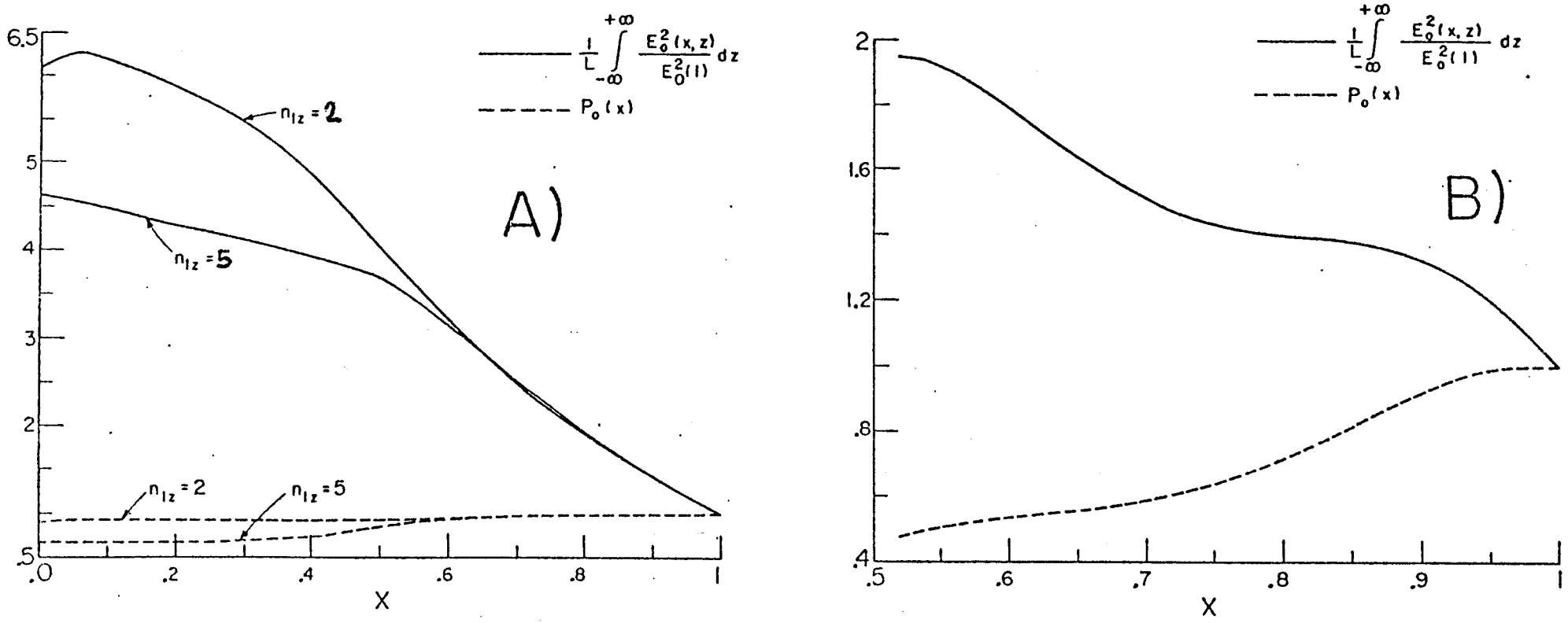
6.5
5
4
3
2
.5
.0
.2
.4
.6
.8
1
X
$\frac{1}{L}\int_{-\infty}^{+\infty} \frac{E_0^2(x,z)}{E_0^2(1)} dz$
$P_o(x)$
$n_{1z}=2$
$n_{1z}=5$
A)
$n_{1z}=2$
$n_{1z}=5$
2
1.6
1.2
.8
.4
.5
.6
.7
.8
.9
1
X
$\frac{1}{L}\int_{-\infty}^{+\infty} \frac{E_0^2(x,z)}{E_0^2(1)} dz$
$P_o(x)$
B)

FIGURE 7

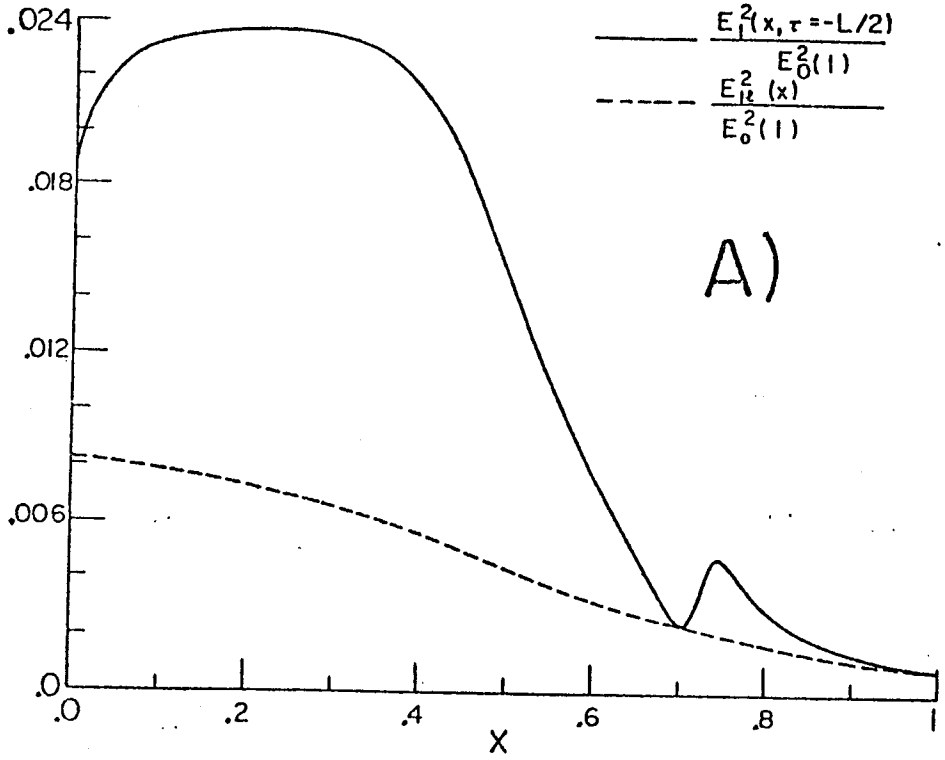
.024
.018
.012
.006
.0
.0
.2
.4
.6
.8
1
X
$\frac{E_1^2(x,\tau=-L/2)}{E_0^2(1)}$
$\frac{E_{1t}^2(x)}{E_0^2(1)}$
A)

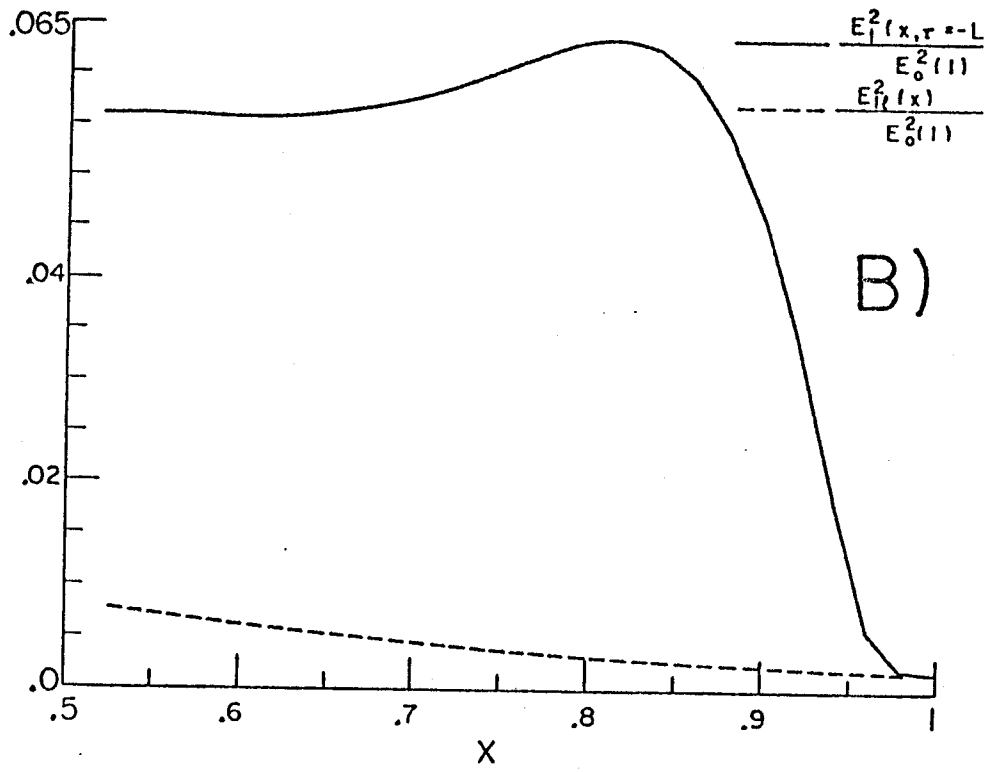
.065
.04
.02
.0
.5
.6
.7
.8
.9
1
X
$\frac{E_1^2(x,\tau=-L}{E_0^2(1)}$
$\frac{E_{1t}^2(x)}{E_0^2(1)}$
B)

FIGURE 8

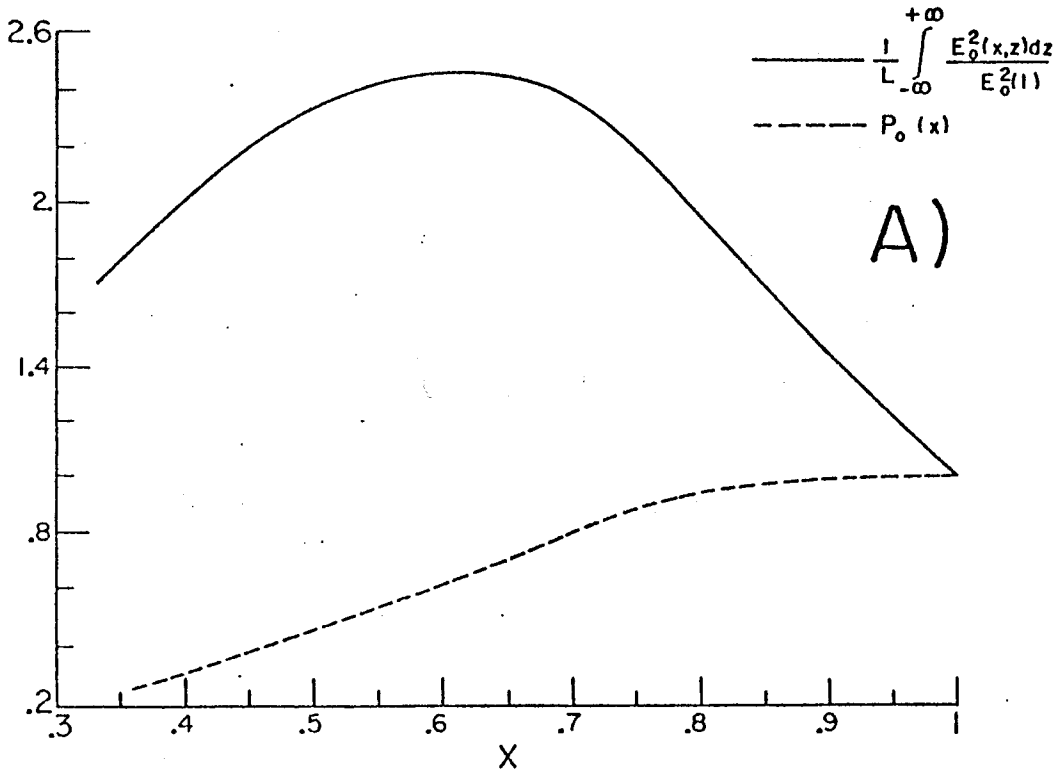
2.6
2.
1.4
.8
.2
.3
.4
.5
.6
.7
.8
.9
1
X
$\frac{1}{L}\int_{-\infty}^{+\infty} \frac{E_o^2(x,z)dz}{E_o^2(1)}$
$P_o(x)$
A)

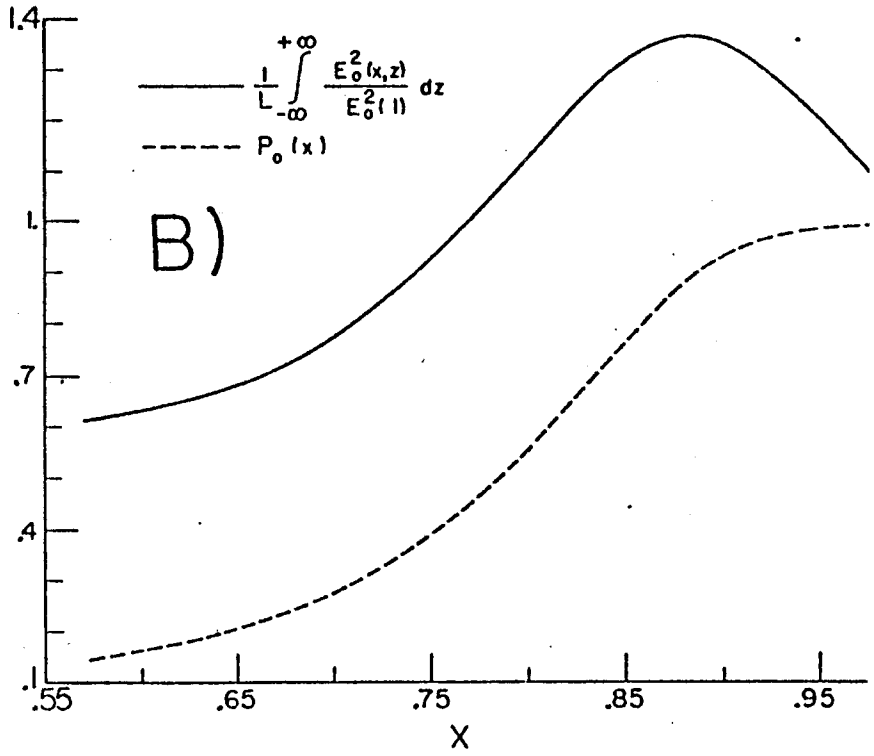
1.4
1.
.7
.4
.1
.55
.65
.75
.85
.95
X
$\frac{1}{L}\int_{-\infty}^{+\infty} \frac{E_o^2(x,z)}{E_o^2(1)}\,dz$
$P_o(x)$
B)

FIGURE 9

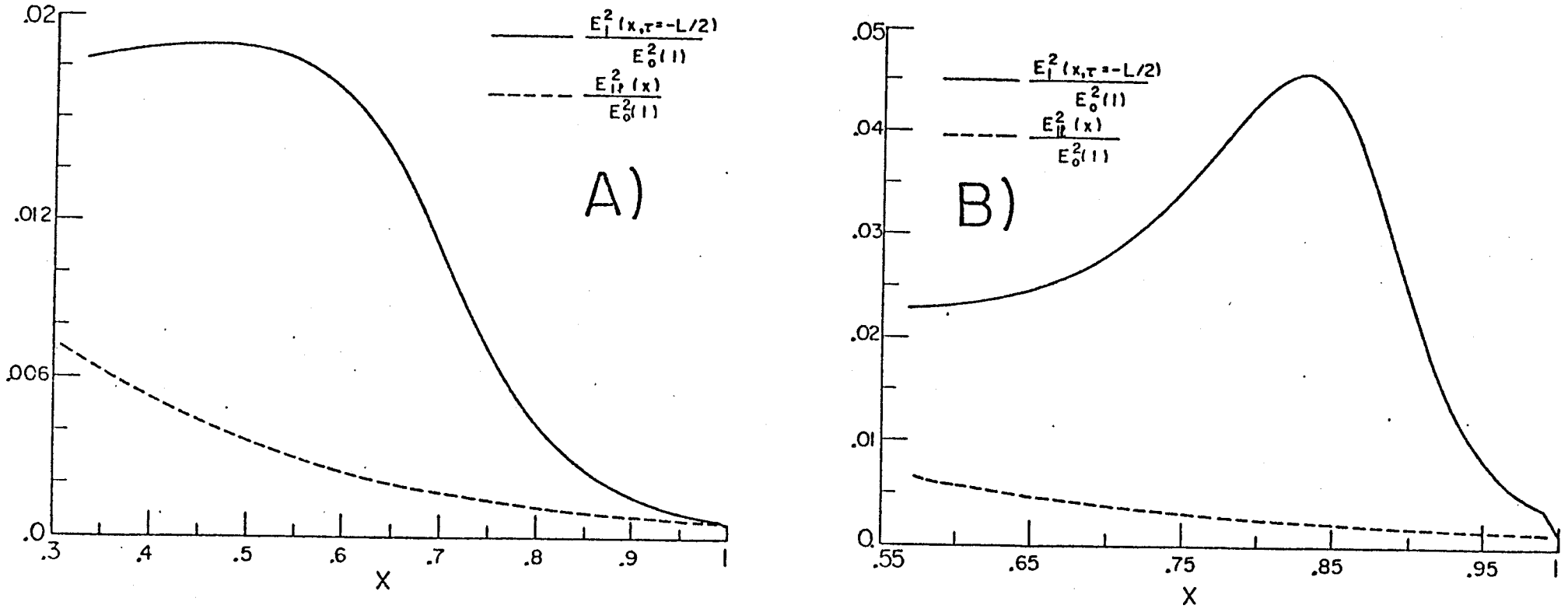
.02
.012
.006
0
.3
.4
.5
.6
.7
.8
.9
1
X
$\frac{E_1^2(x,\tau=-L/2)}{E_0^2(1)}$
$\frac{E_{1P}^2(x)}{E_0^2(1)}$
A)
.05
.04
.03
.02
.01
0
.55
.65
.75
.85
.95
1
X
$\frac{E_1^2(x,\tau=-L/2)}{E_0^2(1)}$
$\frac{E_{1P}^2(x)}{E_0^2(1)}$
B)

FIGURE 10